Polymer Testing 93 (2021) 106888

Contents lists available at ScienceDirect

Polymer Testing

journal homepage: http://www.elsevier.com/locate/polytest

Effect of pre-strain on compression mode properties of magnetorheological elastomers

Hossein Vatandoost *, Ramin Sedaghati, Subhash Rakheja, Masoud Hemmatian

Department of Mechanical, Industrial and Aerospace Engineering, Concordia University, Montreal, QC, H3G 1M8, Canada

ARTICLE INFO

Keywords:
Magnetorheological elastomer
Pre-strain
Compression mode
Dynamic characteristics
Phenomenological model

ABSTRACT

The effects of pre-strain on compression mode dynamic characteristics of both isotropic and aligned magnetorheological elastomers (MREs) are experimentally investigated considering wide ranges of particle volume fraction (15%, 30%, and 45%), frequency (1–30 Hz), and magnetic flux density (0–750 mT) under different levels of pre-strain (6%, 11%, and 21%). Results exhibited strong dependence of MRE behavior on the pre-strain, which was further coupled with the effects of the particle volume fraction and frequency, and the magnetic field. The elastic and loss moduli of isotropic MREs consistently increased in a nonlinear manner, when pre-strain increased from 6% to 21%, suggesting pre-strain stiffening and pre-strain dampening effects, respectively, while aligned MRE showed dissimilar trends depending on particle volume fraction. Results revealed higher pre-strain effects for isotropic MREs than aligned MREs. The relative MR effect in view of elastic modulus ($MR_{E'}$) for both types of MREs consistently decreased with increasing pre-strain, while in view of loss factor (MR_{η}) showed the same trend only for aligned MRE. MR_{η} of isotropic MRE generally showed maximum around 11% pre-strain. Results further revealed maximum $MR_{E'}$, up to 286%, 973% and 2258% for the isotropic MRE, respectively, with volume fraction of 15%, 30% and 45%, and obtained as 320%, 293%, and 386% for aligned MRE. Simple phenomenological models were subsequently proposed to predict the compressive moduli as well as stress-strain hysteresis characteristics of both types of MREs. A reasonably good agreement was observed between the models' results and the experiment data for the ranges of pre-strain, volume fraction, frequency, and magnetic flux density considered. The developed models can be effectively employed for the development and design of controllable MRE-based adaptive devices operating in compression mode.

1. Introduction

Magnetorheological elastomers (MREs) are "intelligent" composite materials, which includes magnetizable particles embedded in a nonmagnetic polymeric matrix. Owing to mutual interaction among ferromagnetic particles in microscopic level, MREs exhibit controllable physical properties in macroscopic scale when an external magnetic field is applied. MREs can be fabricated by mixing micron-sized magnetizable particles in a silicone or natural rubber [1,2]. The magnetizable particles can be spatially dispersed in consistent way (isotropic) or in column-like structures (aligned) inside the medium [3]. The column-like structures in aligned (aligned) MREs can enhance their stiffness and damping properties in comparison with isotropic MREs [4]. The response time for such smart materials to the magnetic field is generally in the order of a few milliseconds [5]. Due to the unique features of MREs, they found to be ideal candidates for numerous engineering applications such as adjustable vibration isolators [6–8], and tunable vibration absorbers [9–11].

To design MRE-based devices, it is crucially important to identify and characterize their dynamic behavior in response to both magnetic and mechanical loadings in different modes of operation. Even though MREs can undergo large deformation in different operational modes, such as shear and compression/extension [12], reported studies have mainly focused on shear mode characterization due to its straightforward experimental procedure in which the mechanical and magnetic force occur in the orthogonal directions [13–16]. Unlike the shear mode, the mechanical and magnetic forces act in the same direction in the compression mode thus the measured force is a combination of both magnetic force, resulted from the two magnetic poles, and the field-dependent viscoelastic force as results of compressing MRE [17]. This makes compensation for the magnetic force, in the compression mode, an essential task. Furthermore, while generation of a controlled

* Corresponding author.
E-mail address: hossein.vatandoost@concordia.ca (H. Vatandoost).

https://doi.org/10.1016/j.polymertesting.2020.106888
Received 20 June 2020; Received in revised form 25 September 2020; Accepted 8 October 2020
Available online 12 October 2020

magnetic field using a reasonable size of the electromagnet is quite difficult challenge in compression mode, rheometers [18] and double-lab shear tests [19] have provided simpler characterization procedures for the shear mode.

Generally, MR effect, determined as relative increase in modulus by increasing the magnetic flux density to maximum level [20,21], in MREs under shear mode, has a tendency to weaken under large strain amplitudes owing to incrementing space between the magnetically attractive particles [22]. MREs in the compression mode, however, show relatively superior MR effect as the particle distances reduce during the compression [23]. Gordaninejad et al. [24] obtained MR effect of nearly 99% in MREs under compression loading compared with 68% observed in MREs under shear loading. Likewise, Lerner and Cunefare [25] developed adaptive vibration absorbers featuring MRE materials and proved that the resonant frequency of the absorbers can shift up to 507% and 470%, in the compression and shear mode, respectively.

Table 1 summarizes recent studies addressing experimental compression mode properties of MREs under different experimental conditions in a chronological order. The maximum MR effect together with the zero-field modulus of the MRE used in each study are also provided in the table. As it can be realized a wide variation in the MR effect, ranging from 8% to as high as 500% has been reported. This difference could be attributed to both the material prescription of the MREs including, size, alignment, and concentration of magnetizable particles as well as the operating conditions such as the driving frequency, pre-strain, strain amplitudes, and range of applied magnetic flux density.

Examination of Table 1 reveals that vast majority of the studies have neither reported nor assessed the effect of pre-strain (or pre-stress) on dynamic behavior of MREs. However, in many applications involving compression of the MRE such as vibration isolators and absorbers, the MRE will likely undergo comprehensive static strain due to weight of the supported structures. The static pre-strain can considerably alter the MR effect due to decrease in the distance between the magnetizable particles. Despite its important significance, very limited studies have been conducted on the effect of pre-strain on the viscoelastic and hysteresis behavior of MREs. Koo et al. [32], Martins et al. [35], and Vatandoost et al. [36] have characterized properties of MREs under specified constant pre-strain of 5%, 6.5%, 0%, respectively. Lee et al. [41] characterized compressive properties of aligned MREs in static regime and showed that lower level of pre-strain in the specimen yielded greater stress adjustments in presence of 300 mT magnetic flux density. Sapouna [37] experimentally assessed the impact of pre-strain on dynamic behavior of MREs at a constant frequency of 5 Hz and obtained 50% and 30% increases in the storage and loss moduli of aligned MRE, respectively, and correspondingly 25% and 5% for isotropic MRE, when pre-strain was increased from 2% to 10%; however, the effect of pre-strain, particularly in a wide range, at various frequencies and higher amounts of magnetic flux density has not yet been investigated.

As it can be realized, reported studies suggest relatively limited knowledge on the impacts of the pre-strain on dynamic features of the MREs in the compression mode. It should be noted that the influences of pre-strain on the properties of filled elastomers are well known. In filled rubbers, an increment in elastic and loss moduli is noted with rising pre-strain [43]. The dynamic properties of MREs are thus expected to depend on the pre-strain. While the pre-strain's impacts on off-state properties of an MRE is comparable to that of a passive filled-elastomer, the dynamic properties of MREs may show significant pre-strain effect in the presence of the magnetic field. Kalina et al. [44] numerically investigated the effect of mechanical pre-load on deformation dependent properties of structured (aligned) and unstructured (isotropic) MREs employing a microscale continuum method. They showed that by varying the pre-load, various impacts can happen on the basis of the microstructure of MREs, predominately, the reciprocal interacting among magnetic particles in curvy chains, which is accountable for their macroscopic reactions such as magnetostriction strain. Besides, the MR effect, which highly relies on the local spatial distribution of magnetizable particles [45], apart from particle volume fraction, is highly dependent on the pre-strain as it can considerably alter the distance between the magnetizable particles.

Considering above, the effect of pre-strain is of paramount importance as it significantly affects the viscoelastic properties of MREs and

Table 1
Summary of studies reporting compression mode characterization of MREs.

Lead author and year	Pre-strain (%)	Magnetic flux density (T)	Maximum MR effect (%)	Frequency (Hz) or rate (mm/min)	Strain (%)	Zero-field modulus/ stiffness	Isotropic/ Aligned	Particle size (μm) and concentration (%) (volume (v) or weight (w))
Bellan [26], 2002	–	0–0.052	100	5 Hz	4–5	4.1 Mpa	Both types	2, soft, 5–30 v
Farshad [27], 2005	–	0–0.44	101	1 mm/min	30	0.427 Mpa	Isotropic	3.8, soft, 80 w
Boczkowska [28], 2007	–	0–0.3	100	5 mm/min	1	0.16 Mpa	Both types	6-9, soft, 1.5–33 w
Fuchs [29], 2007	–	0–0.4	500	0.5–45 Hz	0.1–8	4 Mpa	Both types	3-7, soft, 50–70 w
Kallio [30], 2007	–	0–0.87	11	0.5–15 Hz	1–10	920 N/mm	Both types	3-5, soft, 30 v
Fuchs [31], 2010	–	0–0.62	17	–	20	–	Aligned	3-7, soft, 70 w
Koo [32], 2010	5	0–0.6	38	0.1–1 Hz	5	3 Mpa	Isotropic	10, soft, 30 v
Gordaninejad [24], 2012	–	0–1.6	99	Static	20	0.67 Mpa	Aligned	2-8, soft, 30–70 w
Liao [33], 2012	–	0–1.1	–	–	1–5	–	Both types	6, soft, 80 w
Li [23], 2013	–	0–0.1	10–15	0.1–100 Hz	0.5–5	2.6 Mpa	Aligned	15, soft, 10–30 v
Liao [34], 2013	–	0–0.4	22.7	3200–5600 Hz	1–14	4.09 Mpa	Aligned	2-9 soft, 60–80 w
Schubert [22], 2015a	–	0–0.450	111	10 mm/min	50	2.05 Mpa	Both types	3.7–4.7, soft, 0–30 v
Martins [35], 2017	6.5	0–0.6	10	1–10 Hz	1.5	4000 N/mm	Aligned	-, soft, 30 v
Vatandoost [36], 2017	0	0–0.260	500	0.1–8 Hz	2–14	0.25 Mpa	Isotropic	3-5, soft, 70 w
Sapouna [37], 2018	2–10	0–0.5	28	5 Hz	0.25–2	12 MPa	Both types	(6, 220), soft, 30 v
Agirre-Olabide [38], 2018	–	0–0.085	8	50-200] Hz	0.1–0.7	–	Isotropic	1.25, soft, 0–30 v
Wan [39], 2018	–	0–0.5	30	1–60 Hz	1	23.5 Mpa	Aligned	5-9, soft, 30 v
Bellelli [40], 2019	–	0–0.2	–	1 mm/min	5–10	4.1 Mpa	Both types	45, soft, 20–80 w
Lee [41], 2019	3–18	0–0.3	15	1 mm/min	Up to 20	1–2 Mpa	Aligned	3-10, soft, 29–44 w
Shi [42], 2020	–	0–1	45.9	1–5 Hz	8–10	510 N/mm	Aligned	3-5, soft, 30 v

"-": Not reported.

thus should be considered in the design of MRE-based devices, operating in compression mode. This work aims at thorough experimental examination of the impact of pre-strain on the dynamic compression mode characteristics of both isotropic and aligned MREs comprising different particle volume fraction under varied frequency and magnetic flux density. The force-deflection features of isotropic and aligned MRE samples, manufactured with 15%, 30%, and 45% volume fraction of iron particles, were acquired under harmonic excitation with strain amplitude of 2.5% superimposed on three different pre-strains, including 6%, 11%, and 21% at diverse frequencies varying from 1 to 30 Hz, and magnetic field density up to 750 mT. The experimental data were subsequently scrutinized to assess the effect of pre-strain on the

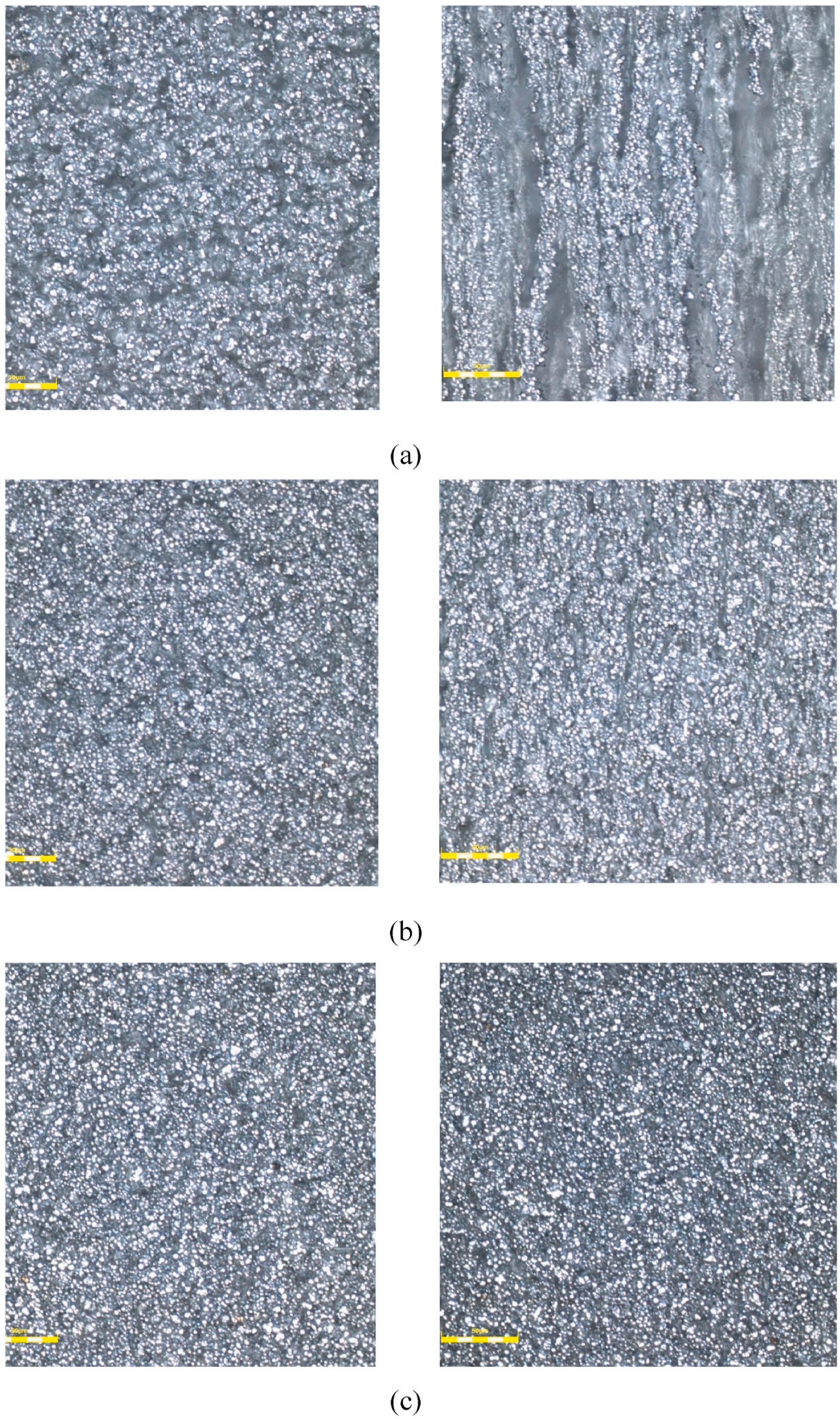

Fig. 1. Microstructure images of fabricated isotropic (left column) and aligned (right column) MREs samples taken by Confocal microscopy with 50X magnifications: (a) 15% volume fraction, (b) 30% volume fraction, and (c) 45% volume fraction.

compression moduli and loss factor of the isotropic and aligned MREs, apart from relative MR effect. A novel physically motivated phenomenological-based model is afterward proposed to predict the compression mode elastic and loss moduli as well as stress-strain hysteresis loops of both types of MREs as functions of the pre-strain, volume fraction, driving frequency and magnetic flux density. The study should provide guidance for potential applications of MREs in vibration isolators and absorbers, where the pre-strain plays an important role.

2. Experimental methods

2.1. MRE specimens

Several isotropic and aligned MRE batches with 15%, 30%, and 45% volume concentrations of carbonyl iron particles (CIPs), corresponding to 56.5%, 76%, and 86% mass faction of CIPs, respectively, were fabricated in the laboratory. The spherical magnetically soft CIPs (SQ, BASF Inc., Germany), with diameter varying from 3.9 to 5 μm were embedded inside a very stretchable platinum-based silicone elastomer (Eco-Flex 00–20, Smooth-On Inc., USA) as the medium. The complete fabrication procedure is presented in Ref. [17]. In a nutshell, the CIP were initially added to the medium and then thoroughly blended using a mixer for around 5 min. The blended mixture was then degasified in a vacuum apparatus for almost 5 min under negative pressure of 736 mmHg, and then slowly placed into two molds, made of cylindrical plexiglass (radius = 50 mm; thickness = 8 mm). One of two batches was allowed to cure for almost 24 h at room temperature, whilst the other batch was cured for 3 h within a homogenous magnetic flux density of 1200 mT, provided by an adjustable air gap electromagnet. Subsequently, several cylindrical MRE specimens with diameter and thickness of 18 mm and 8 mm, respectively, were cut from both batches. The dimension of MRE specimens were chosen in accordance with the current standards for compression testing of rubber-like materials (ISO 7743 [46]). It is noted that the aligned MRE samples were vertically cut parallel to the chain orientation of magnetic particles.

The distribution of magnetic particles inside MREs was evaluated utilizing an engineering laser confocal microscope (OLYMPUS LEXT OLS4000). In this regard, the MRE specimens were vertically sliced parallel to chain orientation employing a scalpel, and then placed under the microscope. Fig. 1 demonstrates the microstructure of both MREs with various particle volume fractions. The white spots in the pictures are the iron particles and the grey backdrop demonstrates the medium of the isotropic (left column) and aligned (right column) MRE specimens. For the isotropic and aligned MREs, correspondingly, homogeneous distribution of particles and the chains of particles in the medium can be clearly observed. Fig. 1 further reveals that the aligned chains, however, are more noticeable for relatively lower level of particle volume fraction.

2.2. Test rig

A test apparatus was custom-built to identify pre-strain dependent characteristics of MREs with different particle volume fraction (15%, 30%, and 45%). The experimental test setup has been extensively elaborated in Ref. [17]. In summary, the setup contained a U–I design of a compact electromagnet, which allowed application of magnetic flux density of up to 1T in the compression direction of the MRE. Two identical MRE specimens, either two isotropic or two aligned MRE specimens, were bonded to the U- and I-form cores of the electromagnet as displayed in Fig. 2, which were fixed on the actuator of a material testing system. The U-shaped core of the electromagnet was connected to the actuator shaft and the I-section was linked to an immovable beam via a 9 kN load cell. The experiments were performed employing the regulated techniques outlines in ISO 7743 [46] for characterizing force-displacement (stress-strain) characteristics of each type of MRE specimen subject to harmonic excitations with strain amplitude (ε_0) of 2.5% superimposed on different static pre-strains. Hence, the pre-strain applied prior to the harmonic compression excitations. While, there is no specific level of static pre-strain have been suggested for dynamic testing of rubbers [47,48], the levels of static pre-strains should be selected such a way that the samples stay undamaged during the tests. Staying in compression region ($\varepsilon_p > \varepsilon_0$) was another key factor in selecting the levels of the pre-strains in the present study. Considering this, the static pre-strains were selected as ε_p = 6%, 11%, and 21%. It should be noted that the considered wide range of static pre-strain superimposed by small sinusoidal excitation can be found in numerous applications such as vibration isolators and absorbers, engine mounts and automotive tires, in which such large level of pre-strains are expected and inevitable due to weight of the supported structures by MREs. It is also noted that even though such large static pre-strains may temporarily destroy the filler network, application of magnetic field can easily reconstruct the broken filler network. It is due to the fact that a very soft silicone rubber

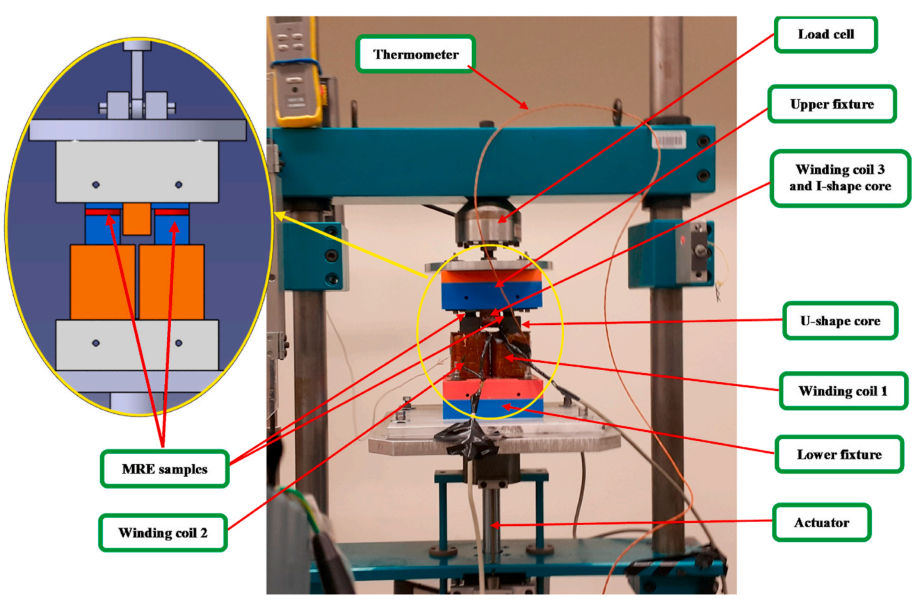

Fig. 2. Pictorial illustration of the test setup for compression mode characterization of the MRE: The red cylinders in the left picture illustrate the position of two MRE samples.

was chosen as the matrix, thereby not only maximizing the relative MR effect but also allowing magnetic particles to easily structure themselves in presence of magnetic field.

Thus, multiple uniaxial experimental tests have been conducted in which the static pre-strain was initially applied and then the harmonic tests were performed on the specimen at different values of magnetic flux density as well as excitation frequencies. Hence, the experiment design involved factorial combinations of three pre-strains (ε_p=6%, 11%, and 21%), applied at four different frequencies (f = 1, 10, 20 and 30 Hz) together with six different amounts of magnetic flux density (B = 0, 150, 300, 450, 600 and 750 mT) on each particle volume fraction (15%, 30%, and 45%) of the MRE specimen, thereby leading to a total of 216 tests. Controlled magnetic flux was realized employing a 1000-Watt power supply. It is noted that the magnetic flux induction within air gap of the electromagnet in absence and presence of MREs were calculated and summarized in Ref. [17]. It should be noted that the force measured during compression mode characterization of an MRE consists of two components: (i) the magnetic pull force generated between I-form and U-form cores of the electromagnet; and (ii) the compression viscoelastic force of the MRE. The force and displacement measurements considering wide range of magnetic flux density were also performed without presence of the MRE specimens within air gap. These measurements were, hence, employed to establish a systematic methodology to precisely predict the magnetic pull force developed by the electromagnet in presence of MRE in the gap [17]. The calculated pull force was deducted from the overall force, recorded by the load cell, in order to extract the field-dependent viscoelastic force of the MRE. The corresponding schematic diagram of the test process and subsequent data analysis are depicted in Fig. 3.

2.3. Data analysis

The force-displacement data were collected in LabView during each trial employing a sampling frequency incrementing from 50 Hz to 5000 Hz, depending on the loading frequency. The steady-state force and displacement data, acquired during four successive oscillation cycles, were low-pass filtered and averaged for subsequent analyses of corresponding stress-strain characteristics, as depicted in Fig. 3. The cut-off frequency of the low-pass filter ranged from 2 Hz to 200 Hz, depending on the loading frequency. By compensating for the magnetic force, the resulting force and displacement data related to compression of MRE subsequently obtained from total force, measured by load cell. These data are, afterward, employed to acquire stress-strain behavior of the MREs, the compression mode elastic (E') and loss (E'') moduli, which represent energy storage and dissipation characteristics of MREs, respectively. The compression moduli are commonly approximated by the slope of the main axis and the closed area of the stress-strain curves, correspondingly, employing peak-to-peak measurement [47] as:

$$E^* = \left|\frac{\sigma_0}{\varepsilon_0}\right| = \sqrt{(E')^2 + (E'')^2} \tag{1}$$

$$E'' = \frac{E_d}{\pi \varepsilon_0^2} \tag{2}$$

where E^*, σ_0, and ε_0, are the complex modulus, maximum stress, maximum strain amplitude. Besides, $E_d = \oint \sigma d\varepsilon$ represents the dissipated energy per cycle which can be obtained from the confined area within the stress-strain curves. Significant inaccuracies may be anticipated for MREs with relatively higher particle volume fraction, which can reveal nonlinearities such as strain-stiffening effect, particularly at the end of loading path in stress-strain characteristics even under relatively lower deformations. Hence, in this study the compression elastic and loss moduli are calculated on the basis of the first harmonic approach using Fourier series of the experimental records, which the ASTM D5992-96 [49] suggests this method for approximating moduli of the rubber-like materials demonstrating nonlinear hysteretic features, as

$$\sigma(t) = \sigma_m + \sum_n \varepsilon_0 \left(E'_n sin(n\omega t) + E''_n cos(n\omega t)\right) \tag{3}$$

whereσ denotes the steady-state output stress and σ_m represents mean stress, corresponding to an applied pre-strain. n, ω, and t represent an integer for indexing number of harmonics, angular frequency and physical time, respectively. The first harmonic moduli, $n = 1$, including E'_1, and E''_1 can be regarded as linear estimation to a nonlinear viscoelastic reaction, which can be visualized as a perfect ellipse (equivalent linear stress-strain characteristic) [50]. To further assess the influences of pre-strain on stress-strain features of both MREs in terms of the energy storage (or equivalent stiffness) and energy dissipation (equivalent damping) characteristics, the 'pre-strain stiffening' and 'pre-strain dampening' effects are defined here on the basis of the estimated first harmonic compression elastic and loss moduli, respectively, from the experimental results as:

$$\%\text{Pre} - \text{strain} - \text{stiffening} = \frac{E'_{\varepsilon_{p\ max}} - E'_{\varepsilon_{p\ min}}}{E'_{\varepsilon_{p\ min}}} \times 100 \tag{4}$$

$$\%\text{Pre} - \text{strain} - \text{dampening} = \frac{E''_{\varepsilon_{p\ max}} - E''_{\varepsilon_{p\ min}}}{E''_{\varepsilon_{p\ min}}} \times 100 \tag{5}$$

where $E'_{\varepsilon_{p max}}$ and $E''_{\varepsilon_{p max}}$ are the compression mode elastic and loss moduli, respectively, corresponding to the maximum pre-strain of 21%.$E'_{\varepsilon_p\ min}$ and $E''_{\varepsilon_p\ min}$ are the reference compression moduli corresponding to the lowest

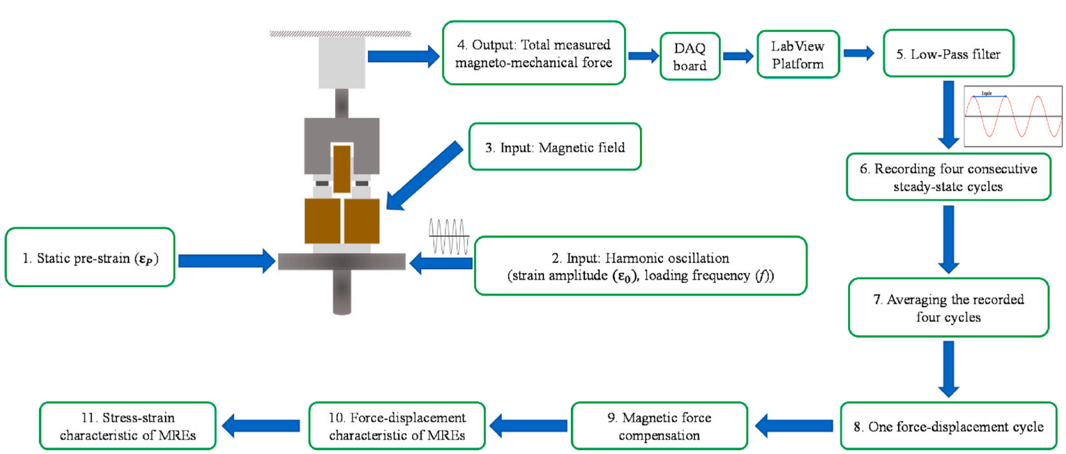

Fig. 3. Schematic diagram of the test process and data analysis.

pre-strain of 6%. To provide a direct and precise description for the test results, all the quantitative results of the linear slope of the main axis and the region bounded by the stress-strain curves, compression mode elastic and loss moduli, loss factor together with the pre-strain stiffening and pre-strain dampening effects for both types of MREs are summarized in Table S1 through Table S11, and Fig. S1 through Fig. S16 in Appendix A. Supplementary Data. It is also noted that the data related to the loading frequency of 20 Hz and 30 Hz for all the pre-strains, particularly, at higher level of flux density could not be obtained considering the high applied current to the electromagnet and safety issue. Therefore, for the sake of consistency, the results related to the loading frequency of 20 Hz and 30 Hz, together with maximum flux density of 750 mT, are just presented in the supplementary data.

3. Experimental results

In the following sections experimental data are analyzed to systematically explore the impact of pre-strain on stress-strain behavior, viscoelastic properties including compression elastic and loss moduli, loss factor as well as relative MR effect of both kinds of MREs.

3.1. Effect of pre-strain on stress-strain properties

The experimental stress-strain features of the isotropic and aligned MREs with different volume fractions, consistently, showed hysteresis phenomenon mostly attributed to viscosity of medium of MREs. Results indicated great dependence of the stress-strain behaviours on the pre-strain, anisotropy, volume fraction, frequency and the magnetic flux density. As an example, Fig. 4 exemplifies the impact of pre-strain on the stress-strain traits of the isotropic and aligned MRE samples with three different volume fractions (15%, 30%, and 45%) subject to harmonic excitation of 1 Hz without presence of the magnetic field. The results exhibit relatively linear viscoelastic behavior in which hysteresis loops are nearly elliptical for both types of MREs, which is more pronounced under the lower levels of pre-strain and volume fraction. Results also revealed that both the main axis slope and the region bounded by the stress-strain hysteresis curve, which can be considered as the equivalent stiffness and damping, respectively, enhance with increasing the pre-strain from 6% to 21%. This behavior is consistent with those previously reported for passive filled-elastomers under uniaxial loading [43].

The particle-matrix and particle-particle interactions are the two main reinforcement mechanisms, that can explain the increase in modulus of filled-elastomers compared to that of unfilled-elastomers

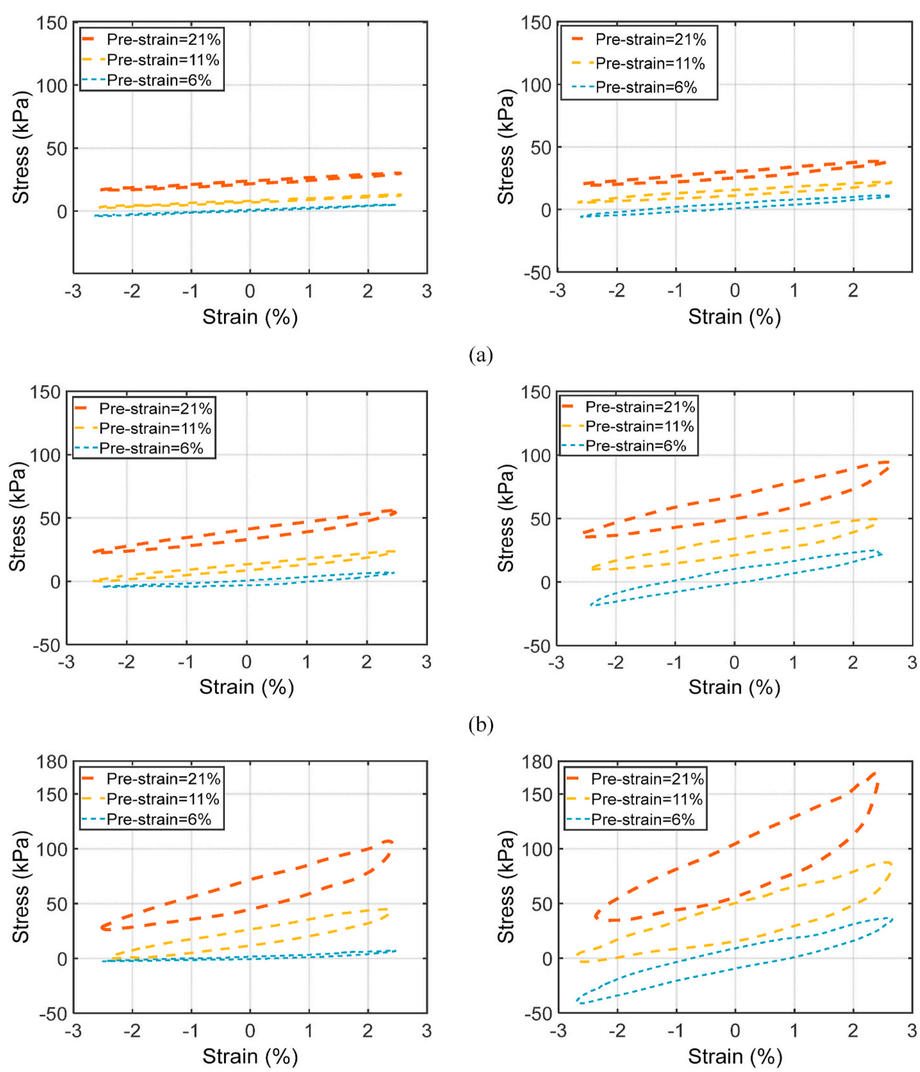

Fig. 4. The effect of pre-strain on the stress-strain features of the isotropic (left column) and aligned (right column) MREs with different particle volume fractions: (a) 15%, (b) 30%, and (c) 45% ($f = 1$ Hz, and $B = 0$ mT).

[51]. The reinforcement mechanisms can be enhanced in a linear and quadratic manner, respectively, for low and high filler volume fraction, taking into account interactions between neighborhood particles [52]. By increasing the static pre-strain, the effective volume faction of filled-elastomer increases due to immobilized occluded [52] and surface-bound [53] elastomeric matrix, thereby, increasing the equivalent stiffness of filled-elastomers. Moreover, the increase in the equivalent damping of filled-elastomers due to increasing pre-strain may be attributed to the enhanced friction between magnetic particles as results of their relative motions to the surrounding elastomeric medium as well as particle-medium interaction [54]. Even though the results presented for the loading frequency of 1 Hz, similar tendency was also observed at the other loading frequencies considered in this study, as can be realized in Tables S1–S3.

Results shown in Fig. 4 also suggest that the impact of pre-strain on the equivalent stiffness and damping becomes more pronounced by incrementing the volume fraction of iron particles, irrespective of loading frequency. Moreover, the stress-strain hysteresis loops move upward with increasing pre-strain which is probably due to the strain amplification effect which enhances the filler-matrix interaction [53]. This tendency has also been reported for passive filled rubber-like materials [63]. Increasing pre-strain from 6% to 21%, yields notably higher peak stress during compression loading as shown in Fig. 4. Results also show that at the zero magnetic flux density, the isotropic MREs revealed higher pre-strain stiffening and pre-strain dampening effects compared to the aligned MREs, irrespective of loading frequency and particle volume fraction, which can also be realized from Tables S4 and S5. This can be ascribed to the lower number of particle-matrix interactivities in aligned MREs in which many particles are close to each other or even aggregated within particle chains, causing lower pre-strain stiffening effect, compared to isotropic MREs. As an example, increasing the pre-strain from 6% to 21% yielded pre-strain stiffening effects of up to 52%, 182%, and 743% for the isotropic MREs with 15%, 30%, and 45% particle volume concentrations, respectively. The corresponding pre-strain stiffening effects for the aligned MRE were found to be 15%, 35%, and 70%. Besides, the corresponding pre-strain dampening effects

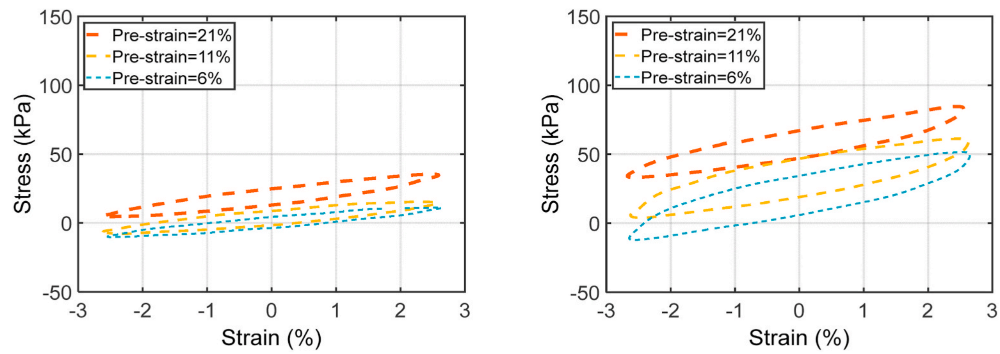

(a)

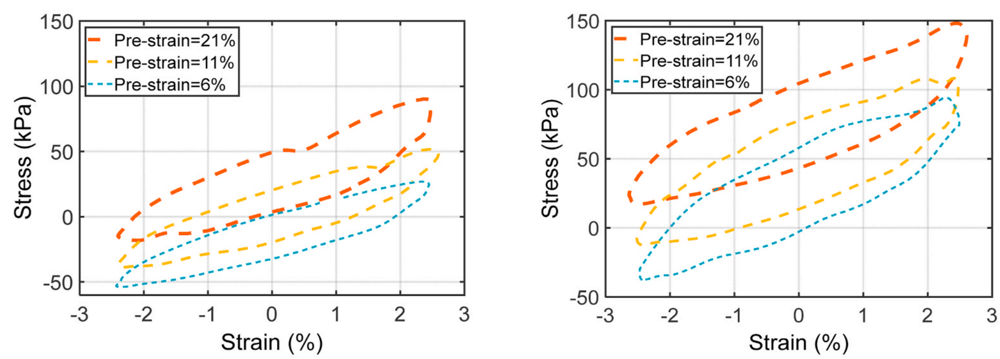

(b)

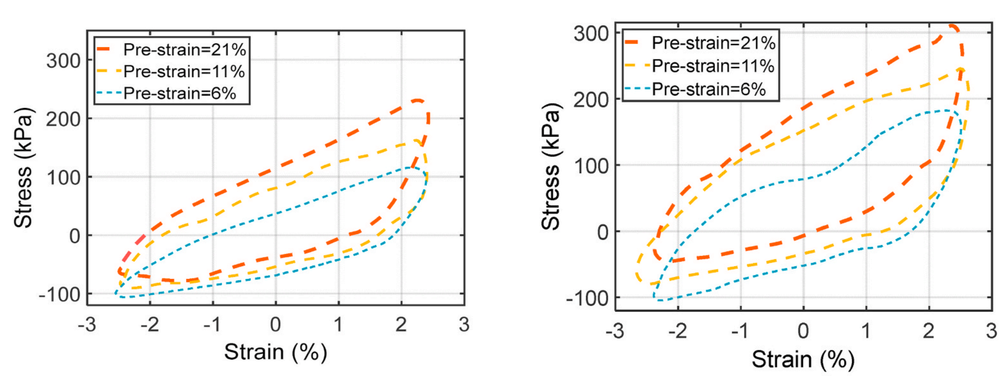

(c)

Fig. 5. The influence of pre-strain on the strain-stress traits of the isotropic (left column) and aligned (right column) MREs with different particle volume fractions: (a) 15%, (b) 30%, and (c) 45% ($f = 1$ Hz, and $B = 450$ mT).

for the isotropic MREs were obtained as 135%, 137%, and 1115% compared with 27%, 74%, and 152% for the aligned MREs, corresponding to 15%, 30%, and 45% particle volume concentrations, respectively.

Fig. 5 demonstrates the impact of pre-strain on the stress-strain properties of both sorts of MREs with three different volume fractions (15%, 30%, and 45%). The results are presented for driving frequency of 1 Hz in the presence of magnetic field ($B = 450$ mT), as example. Fig. 5 shows that pre-strain stiffening effects of both MREs enhances when particle volume fraction increases, which is also observed in absence of field according to Fig. 4. Relatively similar tendency was also observed at the other loading frequencies, as can be realized by Table S4. The results, nonetheless, show that increasing pre-strain from 6% to 21%, generally yielded lower pre-strain stiffening effect for both MREs, when compared with those observed in the absence of the magnetic field (Fig. 4), irrespective of particle volume fraction. This is in part attributed to the fact that the relatively higher pre-strain of 21% causes particles get too close to each other, which becomes more pronounced in presence of magnetic field owing to magnetic attraction, thereby relatively lowering number of dipole-dipole interactions among magnetic particles. The observed decrement in pre-strain stiffening effect, however, is more pronounced for the isotropic MRE due to greater distance between magnetic particles as compared with aligned MRE, thus appearing further susceptible to variation in pre-strain. As an example, for the chosen conditions ($f = 1$ Hz, $B = 450$ mT) and particle volume fraction of 30%, increasing pre-strain from 6% to 21%, yielded relatively lower pre-strain stiffening effects of 26% and −0.3% for the isotropic and aligned MREs, correspondingly, in comparison with those attained without presence of magnetic field, 182% and 35%, respectively.

It is also noted that the observed reduced pre-strain stiffening of both types of MREs, when pre-strain increased from 6% to 21% is not caused by the matrix failure. It is because that the zero-field elastic modulus of both types of MREs consistently increased with increasing pre-strain from 6% to 21%, regardless of loading frequency and particle volume fraction, which can also be realized from Figs. S1, S4, and S7, and also from Figs. S10–S14. However, when pre-strain increased from 6% to 11%, only elastic modulus of the aligned MRE generally decreased, which is due to breaking of filler network. Instead, the magnetic interactions between particles is rather more dominant than polymer elasticity in altering the stiffness of MRE at higher level of pre-strain. More particularly, the very low or negative pre-strain stiffening effect for the aligned MRE in the presence of magnetic field, can mostly credited to this fact that the magnetic particles are already close to each other within chains of anisotropy at relatively lower level of pre-strain (6%), then become too close to each other at higher level of pre-strain (21%). At the same time applying magnetic field causes magnetic particles touch each other, thereby relatively reducing the number of particle-particle interactions or may even disturb the alignment of the particles, and thereby leading to slight softening effect.

Fig. 5 further implies that the negative pre-strain stiffening for the aligned MRE is more observed at lower level of 15% as compared 30% particle volume fraction. It is attributed to comparatively greater distance of iron particle within chains of anisotropy at relatively lower level of particle volume fraction of 15% as compared to 30% according to Fig. 1, thereby becoming more sensitive to alteration in pre-strain. The negative pre-strain stiffening effect has also been observed for an isotropic MRE [56] and aligned MRE [57] in shear mode.

Considering energy dissipation properties, Fig. 5 shows that the pre-strain dampening effect is generally less pronounced in presence of magnetic field in comparison with that in nonattendance of magnetic field, irrespective of particle volume fraction. This is also observed at the other loading frequency, as can be perceived from Table S5. Furthermore, in presence of magnetic field, pre-strain dampening effect for the isotropic MRE is also more pronounced than the aligned MRE, irrespective of particle volume fraction, loading frequency. For instance, for the chosen excitation in Fig. 5, increasing pre-strain from 6% to 21%, yielded 36% and 1% pre-strain dampening effects for the isotropic and aligned MREs with 30% particle volume fraction, respectively, while resulted in 137% and 74% in the zero field. Further examination of results at other loading conditions revealed that pre-strain dampening of the aligned MRE consistently increased with increasing particle volume fraction, irrespective of loading frequency and magnetic flux density, as can also be viewed from Table S5. However, a comparable tendency was not detected for the isotropic MRE, when magnetic field exists.

Fig. 6(a) and (b) illustrate the influence of pre-strain on the stress-strain features of the isotropic and aligned MREs with particle volume fraction of 30% subjected to two different frequencies (1 Hz and 10 Hz), as examples. Results, presented for $B = 600$ mT, suggest that increasing pre-strain from 6% to 21% yields relatively minimal effect on the stress-strain properties of both MREs in terms of linear slope (equivalent stiffness), when frequency increases from 1 Hz to 10 Hz. More particularly, the pre-strain stiffening effect of the isotropic MREs slightly increases as frequency increases, while the aligned MRE showed very small decrement. In general, relatively similar trends were found at the other level of magnetic flux density, as can be noted from Table S4. Fig. 6 further revealed that pre-strain's impact on energy dissipation characteristics of both MRE is comparatively less pronounced, when frequency increased from 1 Hz to 10 Hz. Similar tendency was also seen at other flux density only for the aligned MRE.

Further examination of the results at the other particle volume fraction in presence of magnetic field , revealed that pre-strain stiffening of the isotropic MRE with 15% particle volume fraction tends to decrease with increasing loading frequency, while the 45% isotropic MRE increases with loading frequency in a general manner, irrespective of level of magnetic flux density, according to Table S4. On the other hand, pre-strain stiffening for aligned MRE is slightly increased with increasing loading frequency in a general manner, irrespective of particle volume fraction and magnetic flux density. Furthermore, results showed that pre-strain dampening of the isotropic MRE with particle volume fraction of 15% consistently decreased with increasing driving frequency, while generally increased when particle volume fraction exceeds 15%. Pre-strain dampening for aligned MRE with 15% and 30% generally showed decrement with increasing driving frequency only when flux density exceeds 150 mT, whereas 45% aligned MRE revealed increment with incrementing loading frequency, as can be noticed from Table S5.

3.2. Influence of pre-strain on the compression elastic and loss moduli

The impact of pre-strain on the dynamic viscoelastic characteristics of the isotropic and aligned MREs in the compressive loading are further evaluated in the form of the elastic modulus (E'), loss modulus (E''), and the loss factor (η), which the latter is described as a fraction of the loss modulus over the elastic modulus, by presenting Figs. 7 and 8 related to the particle volume fraction of 30%. It is noted that the specific data associated with the compression moduli at all the loading conditions and particle volume fractions are summarized in Tables S6–S8 in Appendix A. Supplementary Data. Fig. 7 illustrates the effects of pre-strain on behavior of the compression moduli and loss factor of the two isotropic and aligned MREs, as examples, at distinct driving frequencies (1, and 10 Hz) under magnetic flux density of 150 mT. Results display that the elastic modulus of the isotropic MRE rises in a nonlinear way with increasing pre-strain, ranging from 6% to 21%, independent of excitation frequency, which is consistent with the pre-strain stiffening effect observed in the stress-strain characteristics (Figs. 4 and 5). For the aligned MRE, however, the elastic modulus slightly decreases with rising in the pre-strain from 6% to 11%, and then rises with further increment in the pre-strain from 11% to 21%, notwithstanding the driving frequency. Quite comparable trend has also been detected but for an isotropic MRE with 33% particle volume fraction in shear mode in which the MRE at first softens before it become stiff [56]. The initial decrease in the elastic modulus of aligned MRE can be in part credited to the

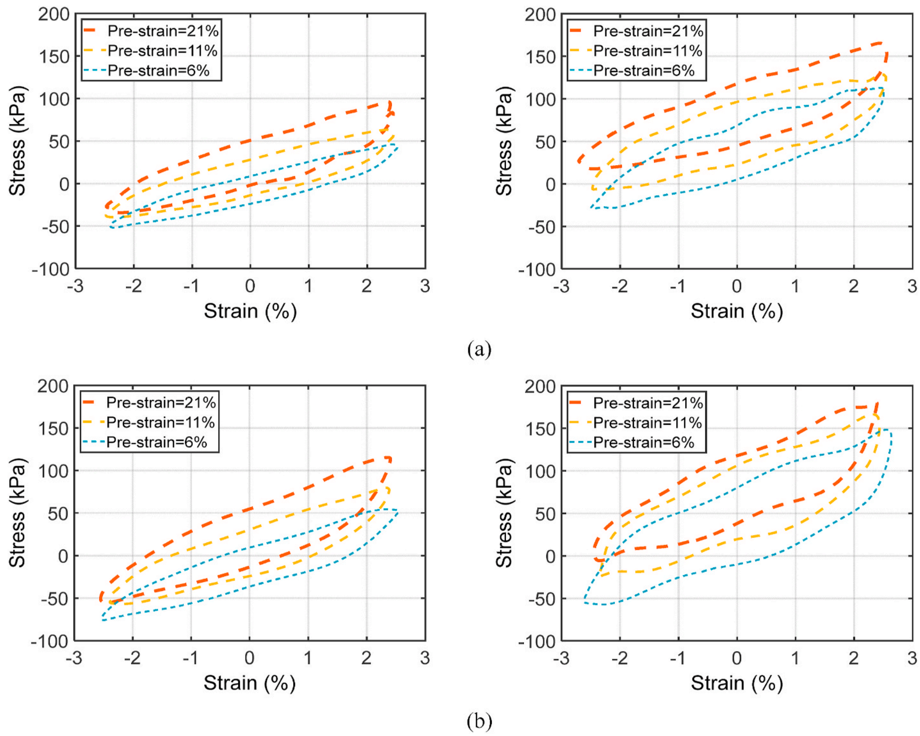

Fig. 6. Effect of pre-strain on stress-strain characteristics of the isotropic (left column) and aligned (right column) MREs with 30% volume fraction under magnetic flux density of 600 mT subject to different frequencies: (a) $f = 1$ Hz, (b) $f = 10$ Hz.

breaking of particle network, thereby reducing the binding of the medium to the particle network. While the increment in the elastic modulus of aligned MRE at higher pre-strain is likely due to greater compression of the trapped medium within the anisotropic chains, apart from slight increasing in the effective volume fraction of filled rubbers, like MREs, under increasing pre-strain [53].

Fig. 7(b) shows that the loss modulus of the isotropic MREs rises with incrementing pre-strain, without regard to loading frequency. This tendency has also been observed for an isotropic MRE foam subjected to frequency of 10 Hz, when compressive pre-strain increased from 35% to 50% [58]. The loss modulus of the aligned MRE, nevertheless, shows comparable results under increasing pre-strain at lower frequency of 1 Hz, while decreases with increase in the pre-strain when loading frequency exceeds 1 Hz. It should be mentioned that a decrement in the loss modulus of chloroprene rubbers by increasing the pre-strain superimposed by a small uniaxial compression oscillation has also been noticed [59]. Chloroprene rubbers are synthetic rubbers like the employed silicone elastomer for fabrication of the examined MRE specimens in this study.

Fig. 7(c) demonstrates that rising pre-strain from 6% to 21% yields pretty comparable loss factor for the isotropic MRE, while loss factor of the aligned MRE increases within (6%–11%) pre-strain range and then decreases with further increment of pre-strain from 11% to 21%. Examination of the results at the other flux densities showed that the loss factor of the isotropic MRE also showed trends similar to that of the aligned MRE, when magnetic flux density exceeds 150 mT. Even though the results in Fig. 7 were presented for specific loading conditions, comparatively same patterns were also noted at the other level of magnetic flux density and driving frequency, as can be noted from Figs. S4–S6 and Table S7, respectively, in Appendix A. Supplementary Data.

Fig. 8 illustrates changes in the elastic and loss moduli of both types of MREs with particle volume fraction of 30% under increasing pre-strain considering various degrees of the magnetic flux density. The outcomes are displayed, as example, at a frequency of 1 Hz. As it shows, the elastic modulus of the isotropic MRE continuously increases with the pre-strain, irrespective of magnetic flux density. The elastic modulus of aligned MRE, however, firstly decreases with increasing pre-strain from 6% to 11% and subsequently enhances with increment of pre-strain from 11% to 21%, which is consistent with the observed trends in Fig. 7. Results also show that the loss modulus of the isotropic MRE increases with rising pre-strain, while the aligned MRE generally reveals comparable loss modulus under increasing pre-strain, irrespective of magnetic flux density, as can be viewed in Fig. 8(b). However, zero flux density formed an exception, where only the aligned MRE shows slight increment within 6%–21% pre-strain range. Further examination of the results revealed that the effect of pre-strain on the elastic and loss moduli of both MREs generally decreases with rising in magnetic flux density, thereby suggesting coupled pre-strain and magnetic field effect on the performance of MREs. This trend is also consistent with the stress-strain hysteresis findings presented in Figs. 4 and 5. By increasing pre-strain from 6% to 21%, for instance, the elastic modulus of the isotropic MRE increases from about 0.22 MPa to 0.62 MPa in the absence of magnetic field, corresponding to 182% increase. In the presence of magnetic field ($B = 450$ mT), the elastic modulus of the isotropic MRE increases from about 1.44 MPa to nearly 1.81 MPa, corresponding to 26% increment.

Fig. 8(c) indicates that the loss factor of both MREs generally increases when pre-strain increased from 6% to 11% and tends to decrease with further increment in pre-strain from 11% to 21%, regardless of magnetic flux density. Loss factor for the isotropic MRE, however, shows relatively comparable trends within the range of pre-strain at comparatively lower level of magnetic flux density compared to the aligned MRE, which is consistent with the observed outcomes illustrated in Fig. 7(c). Furthermore, the elastic modulus of the two kinds of MREs increases significantly with rising in the magnetic flux density up to 600 mT. The rate of enhancement in the modulus, however, relatively reduces when the magnetic flux density exceeds 450 mT, which is ascribed to the magnetic saturation of the MREs with incrementing magnetic flux density. The results shown in Fig. 8(b) also reveal that the loss modulus

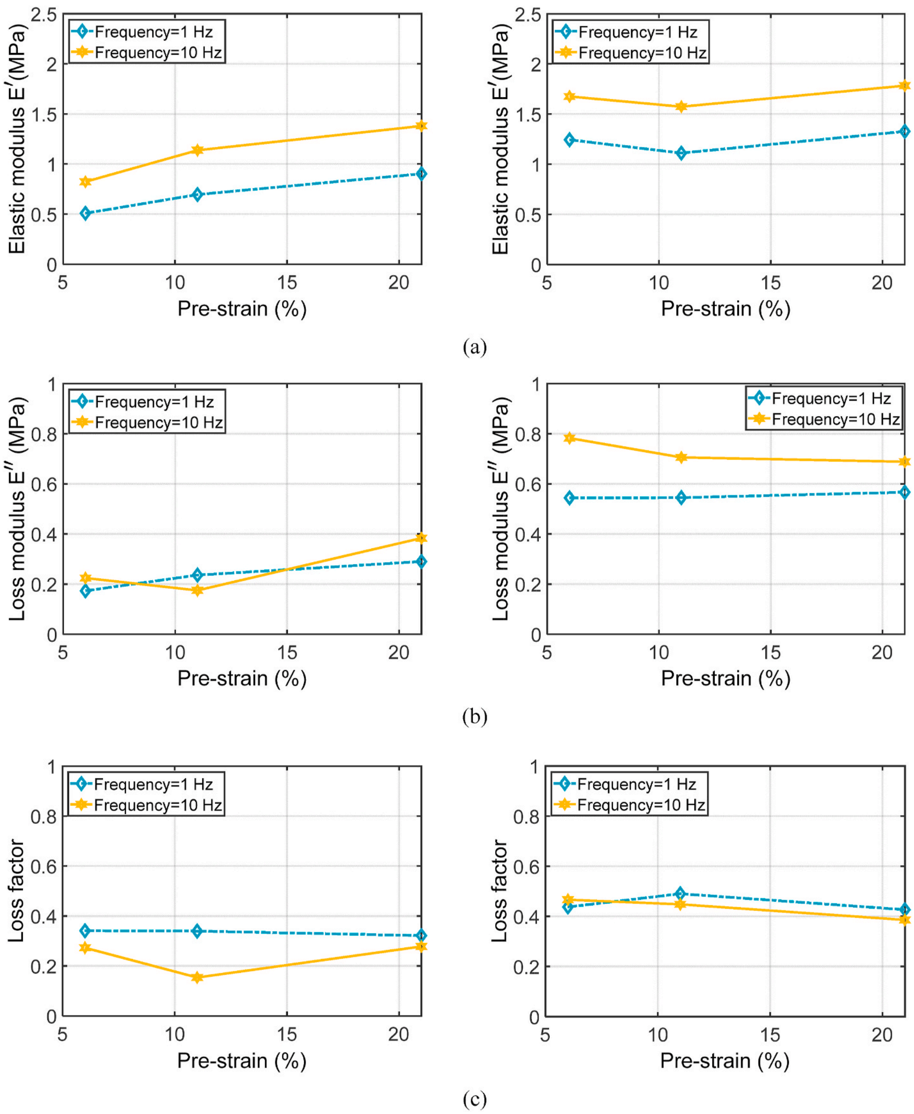

Fig. 7. Influence of pre-strain on the compression mode elastic modulus (a), loss modulus (b), and loss factor (c) of the isotropic (left column) and aligned (right column) MREs with volume fraction of 30% under different excitation frequencies (B=150 mT).

of the aligned MRE is fairly getting close to each other for fields above 450 mT. This implies that the loss modulus of the aligned MRE starts to show tendency to saturate, irrespective of pre-strain. The tendency for magnetic saturation is, however, more pronounced for the loss factor of both kinds of MREs, when magnetic flux density exceeds 450 mT, as compared with the elastic and loss moduli, as can be realized from Fig. 8 (c).

Although Figs. 7 and 8 present the results for the particle volume fraction of 30%, similar tendencies were also found for compression moduli and loss factor of both types of MREs with particle volume fractions of 15% and 45%, regardless of magnetic flux density and loading frequency as shown in Figs. S1–S3, Figs. S7–S14, as well as Table S6 and Table S8 in Appendix A. Supplementary Data. However, only the elastic and loss moduli of the aligned MRE with 15% particle volume fraction tend to decrease with increase in pre-strain ranging from 6% to 21%, while these moduli unceasingly increased in a consistent manner for 45% aligned MRE with the same increment in pre-strain, regardless of loading frequency and magnetic flux density. Furthermore, the pre-strain effects for the isotropic MRE are more pronounced in comparison with the aligned MRE, irrespective of particle volume fraction, loading frequency, magnetic flux density. Moreover, without presence of magnetic field, both elastic and loss modulus of both types of MREs, consistently increase with increasing pre-strain, regardless of particle volume fraction and loading frequency.

Examination of entire results revealed maximum pre-strain stiffening effects of 53%, 248%, and 743% for the isotropic MREs with volume fraction of 15%, 30%, and 45%, respectively, when pre-strain increased from 6% to 21%, which can be noted from Table S4 in Appendix A. Supplementary Data. These were occurred at zero flux density as expected, according to Fig. 5 through Fig. 8, whilst under excitation of 30 Hz, 10 Hz, and 1 Hz, respectively, for the volume fraction of 15%, 30%, and 45%. The corresponding effects for the aligned MREs were obtained as 30%, 44%, and 70%. These were also happened at zero magnetic field as anticipated, whereas at excitation frequency 30 Hz, 20 Hz, and 1 Hz, correspondingly, for the volume fraction of 15%, 30%, and 45%.

3.3. Impact of pre-strain on the relative MR effect

Further assessments are made to study the influences of pre-strain on magnetic field-dependent properties of the isotropic and aligned MREs in form of relative MR effect, which designates the relative alteration in elastic modulus ($MR_{E'}$) or loss factor (MR_{η}) from the off-state condition to a given or maximum possible flux density [22]. The relative MR effects are calculated considering given excitation conditions (pre-strain

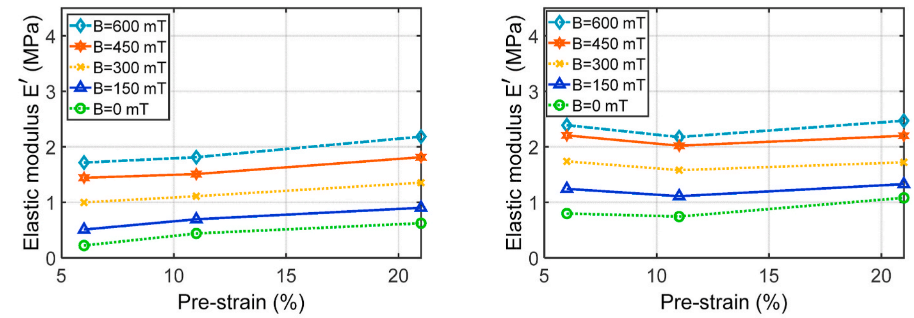

(a)

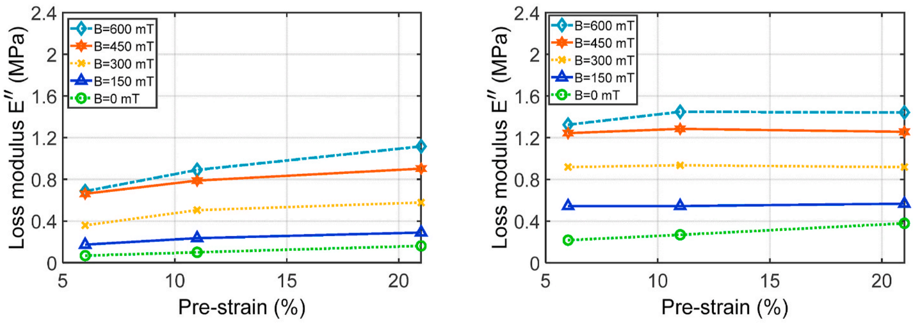

(b)

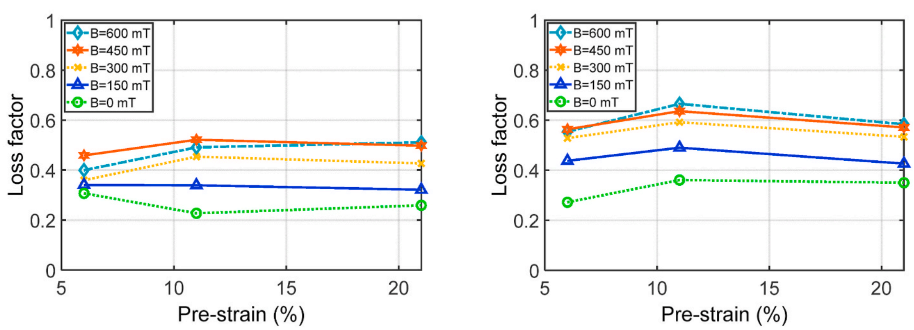

(c)

Fig. 8. Effect of pre-strain on the compression mode elastic modulus (a), loss modulus (b), and loss factor (c) of isotropic (left column) and aligned (right column) MREs with volume fraction of 30% under various degrees of magnetic flux density ($f = 1$ Hz).

and frequency), and different maximum flux densities. It is noted that the specific data related to relative MR effects at all the loading conditions and particle volume fractions are summarized in Table S9 through Table S11 together with Figs. S15 and S16 in Appendix A. Supplementary Data. However, as examples, Fig. 9(a) and (b) exemplify variations in $MR_{E'}$ and $MR_{\eta}$of both types of MREs with particle volume fraction of 30% with respect to pre-strain under magnetic flux density of 600 mT considering two levels of driving frequency 1 Hz and 10 Hz. The results suggest nonlinear decrease in $MR_{E'}$ for the isotropic MRE with increasing pre-strain, irrespective of the excitation frequency. This is also consistent with the results presented in Figs. 5 and 8, suggesting coupled pre-strain and field-stiffening of the MREs. The $MR_{E'}$ for the aligned MRE also decreases almost linearly with pre-strain ranging from 6% to 21%, although the decrease is very small to negligible under increasing pre-strain from 6% to 11%, irrespective of loading frequency.

The results presented in Fig. 9(a) is also consistent with the results presented in Figs. 4 and 5, suggesting less magnetic field dependent properties, when particles getting too close or even touch each other at relatively higher level of pre-strain, which is more pronounced for aligned MREs compared to isotropic MREs. Another possible reason is in part attributed to distortion of the column-like structures of particles in the aligned MRE under relatively higher pre-strain, yielding to lowered relative magnetic permeability, thus reducing relative MR effect. This inclination has also been reflected in a small number of researches evaluating compressive elastic modulus subject to static [41] and dynamic loadings [60], which is become more pronounced for comparatively greater level of particle volume fraction of 30% [22,40]. The rate of decrement in $MR_{E'}$ with increase in pre-strain for aligned MREs is less pronounced compared to that for the isotropic MREs. This is mainly due to the existing columnar particle chains in aligned MREs including particles which are already close to each other even under relatively lower level of pre-strain, thereby becoming less sensitive to further increment of pre-strain as compared with the isotropic MRE. This behavior, similarly, can happen for the isotropic MRE under relatively higher level of pre-strain. Fig. 9(a), for instance, proves comparable $MR_{E'}$ for the isotropic MRE under increasing pre-strain from 11% to 21%.

Results further suggest that the $MR_{E'}$ for the isotropic MRE is relatively less sensitive to increase in excitation frequency, when pre-strain ranging from 11% to 21% as compared with (6%–11%) pre-strain range. This is due to the observed nonlinear pre-strain stiffening effect as can be comprehended in Figs. 7 and 8, which limits the strain-rate stiffening effect, defined as stiffening of MREs due to increase in loading frequency, and hence restricts the $MR_{E'}$. Besides, within the 6%–11% pre-

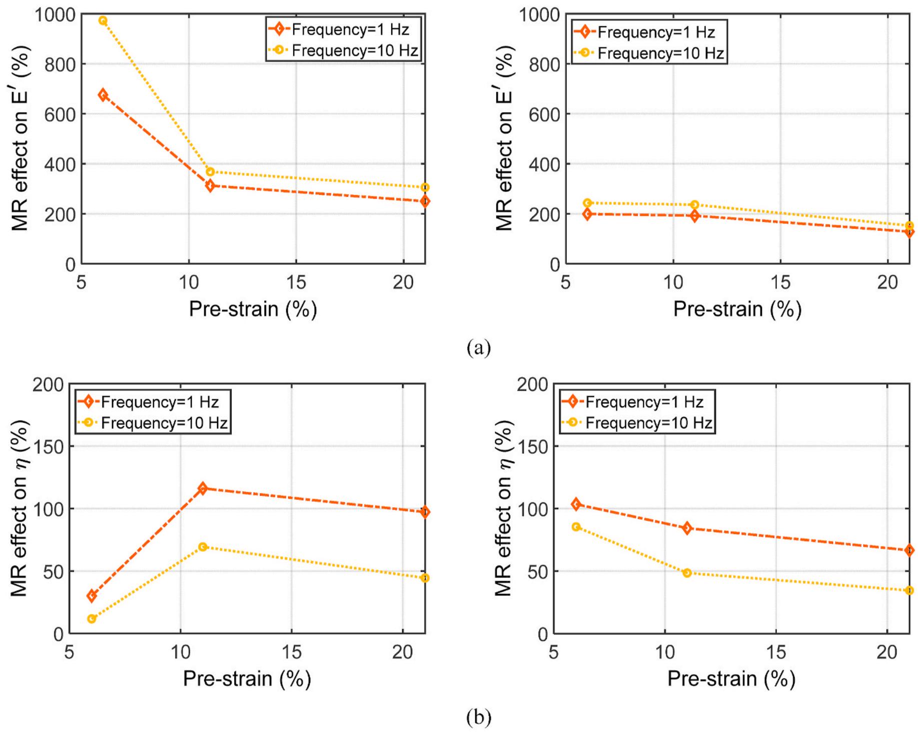

Fig. 9. The effects of the pre-strain on the relative MR effect in sense of elastic (a) and loss factor (b) of the isotropic (left column) and aligned (right column) MREs with 30% volume fraction under different excitation frequencies (B= 600 mT).

strain range, MREs are relatively softer and thus more sensitive to strain-rate stiffening effect, thereby showing stronger dependence of the $MR_{E'}$ on the excitation frequency. This is, however, was not observed for the aligned MRE.

Fig. 9(b) demonstrates that the MR effect in view of loss factor, MR_{η}, for the isotropic MRE shows opposite trends with respect to variations in pre-strain from 6% to 11% as compared with $MR_{E'}$, while decreases with progressive increment of pre-strain from 11% to 21%, irrespective of loading frequency. The MR_{η} of the aligned MRE, however, uninterruptedly reduces with increase in pre-strain rising from 6% to 21%, without being affected by excitation frequency. Further assessment of the attained MR effects at the other loading frequency (20 Hz, and 30 Hz), flux densities varying from 150 mT to 750 mT, and also particle volume fraction (15% and 45%) revealed that both $MR_{E'}$ and MR_{η} for both types of MREs showed similar trends with respect to increase in pre-strain, ranging from 6% to 21%, as shown in Fig. 9, according to provided Tables S9–S11 as well as Figs. S15 and S16 in Appendix A. Supplementary Data. However, loading frequency of 1 Hz when particle volume fraction is 45%, formed an exception where MR_{η} of the isotropic MRE steadily decreases when pre-strain increases from 6% to 21%.

Further examination of the entire obtained MR effects summarized in Tables S9–S11 as well as Figs. S15 and S16 in Appendix A. Supplementary Data, revealed that the aligned MRE with particle volume fraction of 15% revealed higher $MR_{E'}$ in comparison with the isotropic MRE, without regard to pre-strain and loading frequency. Besides, the aligned MRE with particle volume fraction of 45% also revealed higher relative MR effect as against the isotropic MRE, at relatively greater level of pre-strain (11–21%), when loading frequency exceeds 1 Hz, according to Fig. S16 and Table S11 in Appendix A. Supplementary Data. Besides, $MR_{E'}$ of the aligned MRE generally increases with increasing loading frequency, despite of pre-strain and particle volume fraction. Additionally, $MR_{E'}$ of the isotropic MRE with particle volume fraction of 15% also showed increment with increasing loading frequency. However, at particle volume fraction of the 30%, $MR_{E'}$ of the isotropic MRE initially increases with loading frequency from 1 Hz to 10 Hz and then slightly reduces with additional increment in strain-rate from 10 Hz to 30 Hz, in spite of pre-strain, and magnetic flux density. While $MR_{E'}$ of the 45% isotropic MRE generally decreased, when driving frequency rises from 1 Hz to 30 Hz. Moreover, MR_{η} of the isotropic MRE generally drops with growing driving frequency, no matter of pre-strain and particle volume fraction. MR_{η} of aligned MRE with 15% particle volume fraction also decreases with increasing loading frequency, while reveals comparable trends under increasing loading frequency when particle volume fraction exceeds 15%, irrespective of pre-strain.

Additional investigation of the calculated MR effects provided in Tables S9–S11 in Appendix A. Supplementary Data, disclosed maximum $MR_{E'}$ up to 286%, 973% and 2258% for the isotropic MRE with volume fraction of 15%, 30% and 45%, correspondingly. These were obtained at driving strain rates of 10 Hz, 10 Hz, and 1 Hz, in that order, at minimum pre-strain of 6% as expected. The corresponding $MR_{E'}$ for the aligned MREs are found to be 320%, 293%, and 386%, occurred at minimum pre-strain of 6%, and loading strain-rates of 20 Hz, 20 Hz, and 30 Hz, in the same order, for the volume fraction of 15%, 30% and 45%. Results also revealed maximum MR_{η} up to 676%, 1099% and 6645% for the isotropic MREs with volume fraction of 15%, 30% and 45%, respectively. These were observed at excitation frequency of 1 Hz, 10 Hz, 1 Hz, correspondingly, under relatively lower level of pre-strain of 6%, as expected. The corresponding maximum MR_{η} for aligned MREs are also found to be 619%, 537%, and 950%, at excitation strain-rate of 1 Hz, 10 Hz, and 1 Hz, correspondingly, at lower level of pre-strain of 6%.

Further examination of the entire results also suggested that isotropic MREs with 45% and 30% particle volume fraction may be regarded more adapted for designing adjustable MRE-based vibration isolators expose to low (≈1 Hz) and high (≈10 Hz) frequency excitations, in turn, where comparatively greater $MR_{E'}$ is required and at the same time lower level of static pre-strain (≈6%) is unavoidable. Results, likewise, indicated that the aligned MREs are superior compared to the isotropic MREs for designing adaptive MRE-based vibration absorbers, requiring higher payloads with an attempt to track single resonant frequency, where quite lower MR_{η} is desirable, as the lower damping causes higher vibration attenuation for adaptive tuned vibration absorbers [61,62].

4. Model development

In this section, based on the observed experimental data, pre-strain dependent phenomenological-based models have been developed to predict dynamic viscoelastic and nonlinear hysteresis behavior of both isotropic and aligned MREs in compression mode. Apart from the pre-strain effect, the developed models also take into account the variation in the excitation frequency, applied magnetic field as well as volume fraction.

4.1. The compression elastic and loss moduli

In many applications involving MREs under compression mode, such as MRE-based vibration isolators and absorbers, MREs will undergo quite large static pre-strain due to weight of the supported structures, before superimposed by any vibration excitation. As discussed in Section 3, the static strain can considerably alter the MR effect in view of elastic and loss factor due to decrease in the distance between the magnetizable particles as well as changing the shape of specimen. When no magnetic field exists, MREs can be treated like passive filled rubber-like materials. A finite viscoelastic constitutive model has been developed by Hao et al. [63] for estimating the storage and loss moduli of passive filled rubber-like materials in tension mode considering static pre-strain, frequency, and amplitude of excitation. A microscale continuum model has been developed by Kalina et al. [44] which can qualitatively explicate the impact of mechanical preloads on the deformation dependent performance of MREs with orderly and random spatial distribution of the particles. A nonlinear viscoelastic model was developed by Lejon [56] to predict pre-strain dependent properties of isotropic MRE in shear mode under small amplitude of 0.15%. Even though pre-strain is an important design factor in compression mode and has substantial effect on properties of MREs, there is no pre-strain dependent models which can accurately predict the compression elastic and loss moduli together with hysteresis behavior of both isotropic and aligned MREs with different volume fractions considering variation in driving strain-rate and magnetic flux density. Such a model can facilitate the analysis and estimation of the performance of tunable MRE-based vibration suppression mechanisms at early stages of their design.

In the present study, therefore, simple phenomenological models are developed for predicting the pre-strain dependence of the viscoelastic features of the MREs under compression mode. It is noteworthy that the strong effects of the pre-strain on the compression mode properties are also evident from the experimental results, presented in Fig. 4 through 9 in Section 3, which are further coupled with the physical and loading conditions (volume fraction, frequency and magnetic flux density). Apart from volume fraction dependent properties, results further implies that the elastic and loss moduli rise with increase in the magnetic flux density and tend to saturate under higher flux density. Besides, the elastic and loss moduli of the two isotropic and aligned MREs increase with increment in the excitation frequency in a general trend, and mostly show tendency to saturate at relatively higher level of excitation frequency, ranging from 20 Hz to 30 Hz, relatively regardless of particle volume fraction, pre-strain, and magnetic flux density, as can be perceived from Tables S6–S8 in Appendix A. Supplementary Data. Owing to the observed coupled dependence of the elastic and loss moduli on the pre-strain, volume fraction, frequency and magnetic flux density, the effective compression elastic and loss moduli of both isotropic and aligned MREs may be expressed by simple phenomenological-based models as:

$$\begin{cases} E'\left(\varepsilon_p,\varphi,f,\ B\right)=E_0\beta'_0\left(1+\beta'_1\left(\varepsilon_p\right)^{\beta'_2}\right)\left(1+\beta'_3\varphi+\beta'_4\varphi^2\right)\left(1-e^{-\beta'_5 f}\right)\left(\dfrac{2}{1+e^{-\beta'_6 B}}\right) \\ E''\left(\varepsilon_p,\varphi,f,\ B\right)=E_0\beta''_0\left(1+\beta''_1\left(\varepsilon_p\right)^{\beta''_2}\right)\left(1+\beta''_3\varphi+\beta''_4\varphi^2\right)\left(1-e^{-\beta''_5 f}\right)\left(\dfrac{2}{1+e^{-\beta''_6 B}}\right) \end{cases} \tag{6}$$

where E' and E''represents the elastic and loss moduli, sequentially. E_0 is the Young's modulus of the silicone elastomer based medium, taken as 0.0606 MPa [18]. ε_p, φ, f, and B are the static pre-strain, particle volume fraction, loading frequency, and magnetic flux density, respectively. The proposed phenomenological model is based on the multiplicative split of the moduli into a pre-strain dependent, volume fraction dependent, frequency dependent, and magnetic field dependent parts, with only seven parameters. To effectively predict pre-strain, frequency and magnetic field dependent properties, a power function, exponential, and fractional models were proposed, respectively. For volume fraction dependent properties, however, the Einstein-Guth model [64], which can estimate complex modulus of filled rubbers, was employed considering general coefficients. The proposed model involves seven unknown parameters, β'_0 to β'_6 and β''_0 to β''_6, for each elastic and loss moduli, correspondingly, which were determined with minimization of the fault functions J' and J'' between the model-predicted moduli and respective experimentally measured responses as:

$$\begin{cases} J'(a_1,..,a_6)=\sum_{i=1}^{M}\sum_{j=1}^{N}\sum_{k=1}^{O}\sum_{l=1}^{P}\left(E'\left(\varepsilon_p,\varphi,f,\ B\right)-E'_m\left(\varepsilon_p,\varphi,f,\ B\right)\right)^2 \\ J''(a_1,..,a_6)=\sum_{i=1}^{M}\sum_{j=1}^{N}\sum_{k=1}^{O}\sum_{l=1}^{P}\left(E''\left(\varepsilon_p,\ \varphi,f,\ B\right)-E''_m\left(\varepsilon_p,\ \varphi,\ f,\ B\right)\right)^2 \end{cases} \tag{7}$$

where E'_m and E''_m are elastic and loss moduli obtained from the measured data, respectively, and indices *i*, *j*, *k* and *l* denote the experimental data corresponding to specific values of the pre-strain, volume fraction, frequency, and magnetic flux density, respectively. *M*, *N*, *O* and *P* stand for the number of outcomes corresponding to the respective input factors considered in the error function, which were taken as 3, 3, 4, and 5, respectively. The error minimization problem was solved employing the Genetic algorithm (GA) followed by the nonlinear Sequential Quadratic Programming (SQP) technique for the purpose of acquiring precise convergence to global minima, as suggested in Ref. [65]. Repeated solutions were obtained considering different initial values of the coefficients, which all converged to nearly identical solutions, summarized in Tables 2 and 3 for the elastic and loss moduli models, respectively, for both the isotropic and aligned MREs.

Figs. 10 and 11 compare the model-predicted elastic and loss moduli of the isotropic and aligned MREs, respectively, with the experimental records for three distinct values of the pre-strain as well as volume fraction. Figs. 10 and 11 present the comparison under driving frequency and magnetic flux density of 1 Hz and 300 mT and also 10 Hz and 450 mT, respectively, as examples. The comparisons demonstrate that the proposed simple phenomenological models can reasonably well estimate the elastic and loss moduli of both types of MREs with different

Table 2
Identified coefficients of the proposed model for estimating the elastic modulus of both kinds of MREs.

Constant	$\beta_0^{'}$	$\beta_1^{'}$	$\beta_2^{'}$	$\beta_3^{'}$	$\beta_4^{'}$	$\beta_5^{'}$	$\beta_6^{'}$
Isotropic MRE $E^{'}$	9.0739	8.2388	0.8689	−8.2219	25.8811	0.8379	4.7096
Aligned MRE $E^{'}$	11.3866	72.6082	3.8618	−3.6533	22.5994	1.7655	5.0534

Table 3
Identified coefficients of the proposed model for estimating the loss modulus of both kinds of MREs.

Constant	$\beta_0^{''}$	$\beta_1^{''}$	$\beta_2^{''}$	$\beta_3^{''}$	$\beta_4^{''}$	$\beta_5^{''}$	$\beta_6^{''}$
Isotropic MRE $E^{''}$	−227.6527	−1.1122	0.0238	−10.0130	28.2890	1.5030	4.9695
Aligned MRE $E^{''}$	−105.6616	−1.0987	0.0109	−8.4531	35.2759	2.1375	5.2561

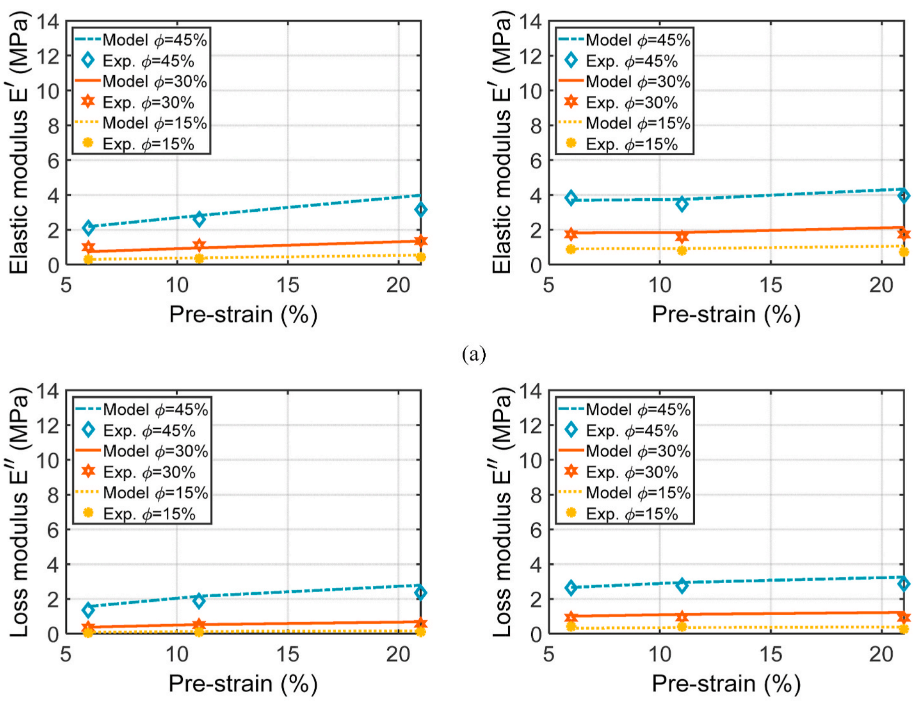

Fig. 10. Comparisons of the pre-strain dependent compression elastic (a) and loss moduli (b) predicted from the proposed model with the measured data for the isotropic (left column) and aligned (right column) MREs with different volume fractions ($f = 1$ Hz, $B = 300$ mT).

particle volume fraction for the range of the pre-strain considered in the study. A quite similar degree of correspondences between the model and measured data were also observed across the full ranges of pre-strain, volume fraction, driving frequency and magnetic flux density examined in this research.

The performance of the proposed models was also evaluated quantitatively using the coefficient of determination , R^2, is a statistical measure to inspect the goodness of fit between the measured and model responses. The R^2 for the models, predicting the isotropic and aligned elastic moduli, were obtained as 93.49% and 87.84%, respectively while were found as 87.40% and 83.99%, for models predicting loss moduli of isotropic and aligned MREs, correspondingly. The root-mean-square error (RMSE) was also calculated as 0.496 and 0.607 for the models predicting the isotropic and aligned elastic moduli, respectively. The corresponding RMSE for the models estimating the isotropic and aligned loss moduli were also found to be 0.411 and 0.571, respectively. These indicate that the proposed pre-strain dependent, volume fraction dependent, frequency dependent, and magnetic field dependent model can fairly well capture the elastic and loss modulus of both types of MREs.

4.2. Stress-strain hysteresis characteristics

In order to predict stress-strain hysteresis traits of the isotropic and aligned MREs subject to harmonic compression deformation, a nonlinear Kelvin-Voigt viscoelastic model was developed in which the stored and dissipated energy elements are lumped and linked in parallel configuration, as shown in Fig. 12. The proposed model represents the steady-state stress output of the MRE in response to a harmonic excitation input as:

$$\sigma_{MRE}(t) = E(\varepsilon_p\,\varphi,\, f,\, B)\varepsilon(t) + \xi(\varepsilon_p,\, \varphi,\, f,\, B)\dot{\varepsilon}(t) \tag{8}$$

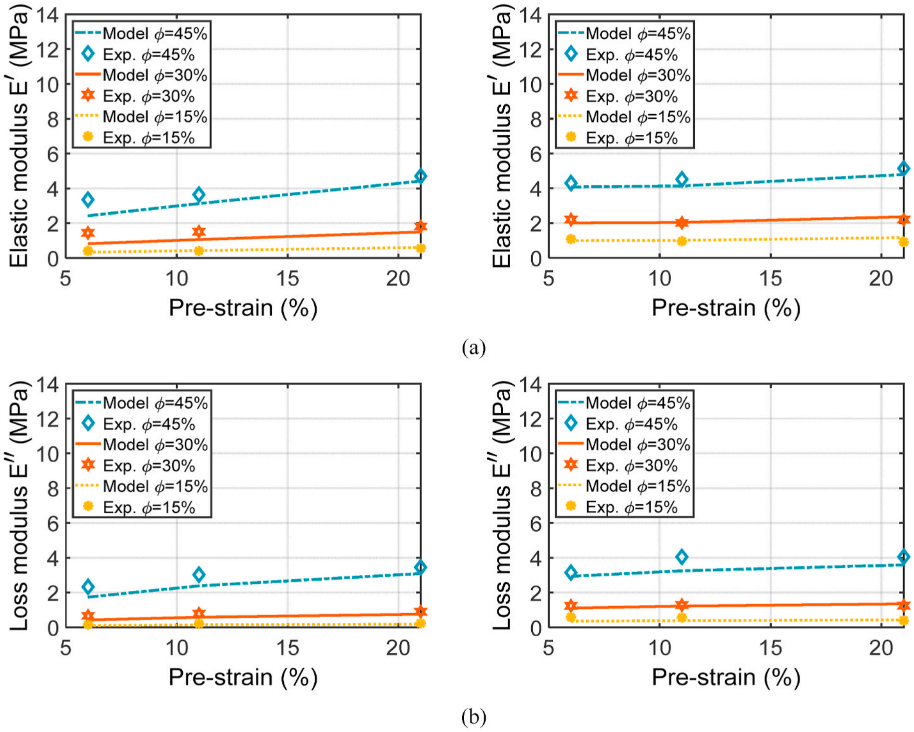

Fig. 11. Comparisons of the pre-strain dependent compression elastic (a) and loss moduli (b) predicted from the proposed model with the experimental data for the isotropic (left column) and aligned (right column) MREs with different volume fractions (f = 10 Hz, B = 450 mT).

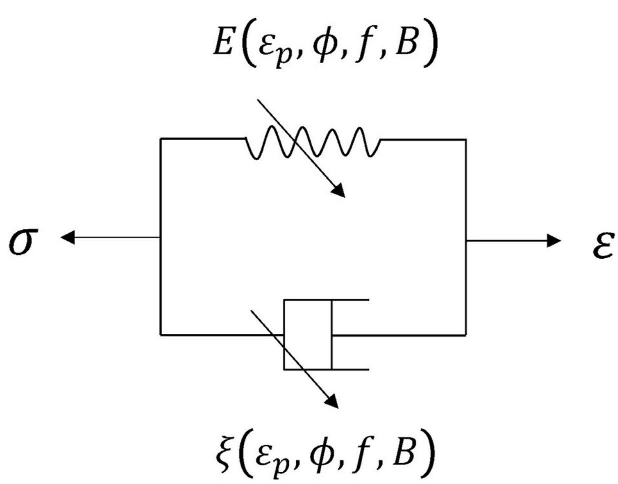

Fig. 12. Nonlinear viscoelastic model for MREs.

where $\sigma(t)$, $\varepsilon(t)$, and $\dot{\varepsilon}(t)$ are the stress, strain, and strain-rate, respectively in which t represents physical time related to harmonic input oscillation. $E(\varepsilon_p,\ \varphi,\ f,\ B)$and $\xi(\varepsilon_p,\ \varphi,\ f,\ B)$, correspondingly, represent the dynamic compression elastic modulus and viscosity of the viscoelastic materials such as MREs. Furthermore, ε_p, φ, f, and B are the static pre-strain, particle volume fraction, excitation frequency, and magnetic flux density, respectively. Let us consider a harmonic excitation under complex strain input $\varepsilon^*(t)$ as:

$$\varepsilon^* = \varepsilon_0 e^{i2\pi ft} \tag{9}$$

where ε_0 is strain amplitude. In the proposed viscoelastic Kelvin–Voigt model, the elastic modulus$E(\varepsilon_p,\ \varphi,\ f,\ B)$and viscosity $\xi(\varepsilon_p,\ \varphi,\ f,\ B)$ can be related to the elastic and loss moduli of the MRE. The complex dynamic modulus, E^* can be used to relate complex stress and strain as:

$$\sigma^* = E^*\varepsilon^* = (E' + iE'')\varepsilon^* \tag{10}$$

where E' and E'' are the compressive elastic and loss moduli, one-to-one. Now considering Eqs. 8–10, the $E(\varepsilon_p,\ \varphi,\ f,\ B)$and $\xi(\varepsilon_p,\ \varphi,\ f,\ B)$ can be expressed with respect to elastic and loss moduli of MREs as:

$$E(\varepsilon_p,\ \varphi,\ f,\ B) = E' \tag{11}$$

$$\xi(\varepsilon_p,\ \varphi,\ f,\ B) = \frac{E''}{2\pi f} \tag{12}$$

Thus, in the proposed nonlinear viscoelastic model presented in Eq. (8), the elastic modulus and viscosity components can be identified using elastic and loss moduli of the MREs formulated in Eq. (6). Fig. 13 illustrates the usefulness of the suggested nonlinear viscoelastic model in forecasting compression mode stress-strain characteristics of both types of MREs, as examples, at two magnetic flux density of 300 mT and 450 mT, considering different loading frequency (1 Hz, 10 Hz, and 30 Hz), and varied static pre-strains (6%, 11%, and 21%). Reasonably well correspondences between the model approximated stress-strain features of both types of MREs and the corresponding measured data were also obtained upon the whole ranges of pre-strain, volume fraction, loading frequency and magnetic flux densities studied in this research.

(a)ε_p=11%,φ=30%, f=10 Hz,B=450 mT (b)ε_p=6%,φ=30%, f=30 Hz,B=300 mT

(c) ε_p=11 %, φ=45%, f=10 Hz, B=300 mT (d) ε_p=21%, φ=45%, f=1 Hz, B=300 mT

5. Conclusion

The results showed strong dependence of the elastic and loss moduli of isotropic and aligned MREs on the pre-strain, which was further coupled with the effects of the volume fraction and frequency, and the magnetic field. The elastic and loss moduli of isotropic MREs consistently increase in a nonlinear manner, when pre-strain increased from 6% to 21%, while aligned MRE showed dissimilar trends depending on

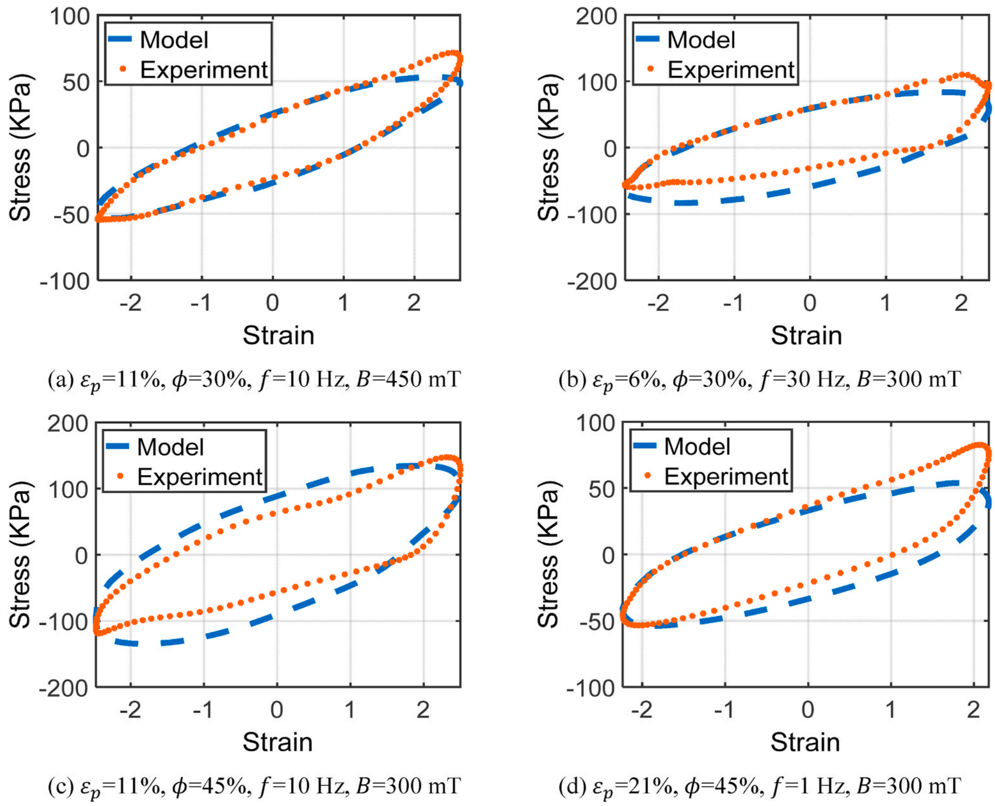

(a) ε_p=11%, ϕ=30%, f=10 Hz, B=450 mT
(b) ε_p=6%, ϕ=30%, f=30 Hz, B=300 mT
(c) ε_p=11%, ϕ=45%, f=10 Hz, B=300 mT
(d) ε_p=21%, ϕ=45%, f=1 Hz, B=300 mT

Fig. 13. Comparisons of the stress-strain hysteresis traits estimated by the proposed model with the experimental records for the isotropic (a, c, and d), aligned (b) MREs subject to different level of pre-strain and excitation conditions.

particle volume fraction. The pre-strain stiffening effect, however, was generally limited in the presence of anisotropy, and magnetic field-stiffening of the MREs, while dramatically enhances with increase in volume fraction, particularly for isotropic MRE. Pre-strain-stiffening and pre-strain dampening effects for isotropic MRE are always more noticeable than aligned MRE. Pre-strain dampening of aligned MRE always increased with increasing particle volume fraction, while isotropic MRE only showed this trend in absence of magnetic field. Both pre-strain effects of isotropic MRE consistently decreased with increasing frequency in absence of magnetic field, while aligned MRE showed similar behavior, when particle volume fraction exceeds 15%, whereas at 15% showed increment with increasing frequency. The relative MR effect considering elastic modulus ($MR_{E'}$) for both types of MRE consistently decreased with increase in pre-strain, which is more evident for the isotropic MRE as opposed to aligned MRE. The relative MR effect pertaining to loss factor (MR_η) showed the same trend only for aligned MRE. MR_η of isotropic MRE generally showed maximum around 11% pre-strain. Results further revealed maximum $MR_{E'}$, up to 286%, 973% and 2258% for the isotropic MRE, respectively, with volume fraction of 15%, 30% and 45%. The corresponding $MR_{E'}$ for aligned MREs obtained as 320%, 293%, and 386%. Results also revealed maximum MR_η, up to 676%, 1099% and 6645% for the isotropic MRE, respectively, with volume fraction of 15%, 30% and 45%. The corresponding MR_η for aligned MREs obtained as 619%, 537%, and 950%. Results also recommended that isotropic MREs with 45% and 30% particle volume fractions may be better suited for designing MRE-based vibration isolators under low (≈1 Hz) and high (≈10 Hz) frequency excitations, correspondingly, when lower level of static pre-strain (≈6%) is inevitable. Results, likewise, indicated that the aligned MREs are relatively superior compared to the isotropic MRE for designing MRE-based vibration absorbers, when relatively higher level of payload is unavoidable. Simple phenomenological models were proposed for predicting pre-strain dependent compression moduli and stress-strain hysteresis characteristics of both kinds of MREs, which showed a reasonably good agreement with the experimental data across the full spectrum of pre-strain, volume fraction, loading frequency, magnetic flux density investigated. The proposed models could thus serve as a guidance for designing MRE-based devices considering different level of pre-strain and volume fraction.

Data availability

The raw/processed data required to reproduce these findings cannot be shared at this time as the data also forms part of an ongoing study.

CRediT authorship contribution statement

Hossein Vatandoost: Conceptualization, Methodology, Data curation, Formal analysis, Software, Validation, Investigation, Visualization, Writing - original draft. **Ramin Sedaghati:** Supervision, Investigation, Validation, Resources, Writing - review & editing, Funding acquisition. **Subhash Rakheja:** Supervision, Investigation, Validation, Resources, Writing - review & editing, Funding acquisition. **Masoud Hemmatian:** Methodology, Visualization, Writing - review & editing.

Declaration of competing interest

The authors declare that they have no known competing financial interests or personal relationships that could have appeared to influence the work reported in this paper.

Acknowledgement

Finacial support from the National Sciences and Engineering Research Council of Canada (NSERC), Grant No. RGPIN/6696-2016, is gratefully acknowledged.

Appendix A. Supplementary data

Supplementary data to this article can be found online at https://doi.org/10.1016/j.polymertesting.2020.106888.

References

[1] A. Dargahi, R. Sedaghati, S. Rakheja, On the properties of magnetorheological elastomers in shear mode: design, fabrication and characterization, Compos. B Eng. 159 (2019) 269–283.
[2] M. Norouzi, M. Gilani, S.S. Alehashem, H. Vatandoost, Dynamic characterization and modeling of isotropic magnetorheological elastomers under tensile-compressive loadings, IEEE Trans. Magn. 53 (9) (2017) 1–12.
[3] G.V. Stepanov, A.V. Chertovich, E.Y. Kramarenko, Magnetorheological and deformation properties of magnetically controlled elastomers with hard magnetic filler, J. Magn. Magn Mater. 324 (21) (2012) 3448–3451.
[4] T. Tian, M. Nakano, Fabrication and characterisation of aligned magnetorheological elastomer with 45 iron particle alignment at various silicone oil concentrations, J. Intell. Mater. Syst. Struct. 29 (2) (2018) 151–159.
[5] M. Zhu, M. Yu, S. Qi, J. Fu, Investigations on response time of magnetorheological elastomer under compression mode, Smart Mater. Struct. 27 (5) (2018), 055017.
[6] G.J. Liao, X.L. Gong, S.H. Xuan, C.J. Kang, L.H. Zong, Development of a real-time tunable stiffness and damping vibration isolator based on magnetorheological elastomer, J. Intell. Mater. Syst. Struct. 23 (1) (2011) 25–33.
[7] S. Yarra, F. Gordaninejad, M. Behrooz, G. Pekcan, A.M. Itani, N. Publicover, Performance of a large-scale magnetorheological elastomer–based vibration isolator for highway bridges, J. Intell. Mater. Syst. Struct. 29 (20) (2018) 3890–3901.
[8] A. Jalali, H. Dianati, M. Norouzi, H. Vatandoost, M. Ghatee, A novel bi-directional shear mode magneto-rheological elastomer vibration isolator, J. Intell. Mater. Syst. Struct. 31 (17) (2020) 2002–2019.
[9] A.A. Lerner, K. Cunefare, Performance of MRE-based vibration absorbers, J. Intell. Mater. Syst. Struct. 19 (5) (2008) 551–563.
[10] H-x Deng, X-l Gong, Application of magnetorheological elastomer to vibration absorber, Commun. Nonlinear Sci. Numer. Simulat. 13 (9) (2008) 1938–1947.
[11] G. Liu, K. Lu, D. Zou, Z. Xie, Z. Rao, N. Ta, Development of a semi-active dynamic vibration absorber for longitudinal vibration of propulsion shaft system based on magnetorheological elastomer, Smart Mater. Struct. 26 (7) (2017), 075009.
[12] H. Vatandoost, S.M.S. Alehashem, M. Norouzi, H. Taghavifar, Y.-Q. Ni, A supervised artificial neural network-assisted modeling of magnetorheological elastomers in tension–compression mode, IEEE Trans. Magn. 55 (12) (2019) 1–8.
[13] T.H. Nam, I. Petríková, B. Marvalová, Experimental characterization and viscoelastic modeling of isotropic and aligned magnetorheological elastomers, Polym. Test. 81 (2020), 106272.
[14] W. Gao, X. Wang, Magneto-elastic properties of isotropic MR elastomers with a tri-modal particle size distribution, Polym. Test. 80 (2019), 106105.
[15] E. Burgaz, M. Goksuzoglu, Effects of magnetic particles and carbon black on structure and properties of magnetorheological elastomers, Polym. Test. 81 (2020), 106233.
[16] I.A. Perales-Martínez, L.M. Palacios-Pineda, L.M. Lozano-Sánchez, O. Martínez-Romero, J.G. Puente-Cordova, A. Elías-Zúñiga, Enhancement of a magnetorheological PDMS elastomer with carbonyl iron particles, Polym. Test. 57 (2017) 78–86.
[17] H. Vatandoost, M. Hemmatian, R. Sedaghati, S. Rakheja, Dynamic characterization of isotropic and aligned magnetorheological elastomers in the oscillatory squeeze mode superimposed on large static pre-strain, Compos. B Eng. 182 (2020), 107648.
[18] M. Asadi Khanouki, R. Sedaghati, M. Hemmatian, Experimental characterization and microscale modeling of isotropic and aligned magnetorheological elastomers, Compos. B Eng. 176 (2019), 107311.
[19] M. Norouzi, S.M. Sajjadi Alehashem, H. Vatandoost, Y.Q. Ni, M.M. Shahmardan, A new approach for modeling of magnetorheological elastomers, J. Intell. Mater. Syst. Struct. 27 (8) (2016) 1121–1135.
[20] M. Lokander, B. Stenberg, Improving the magnetorheological effect in isotropic magnetorheological rubber materials, Polym. Test. 22 (6) (2003) 677–680.
[21] M. Lokander, B. Stenberg, Performance of isotropic magnetorheological rubber materials, Polym. Test. 22 (3) (2003) 245–251.
[22] G. Schubert, P. Harrison, Large-strain behaviour of Magneto-Rheological Elastomers tested under uniaxial compression and tension, and pure shear deformations, Polym. Test. 42 (2015) 122–134.
[23] R. Li, L.Z. Sun, Viscoelastic responses of silicone-rubber-based magnetorheological elastomers under compressive and shear loadings, J. Eng. Mater. Technol. 135 (2) (2013), 021008.
[24] F. Gordaninejad, X. Wang, P. Mysore, Behavior of thick magnetorheological elastomers, J. Intell. Mater. Syst. Struct. 23 (9) (2012) 1033–1039.
[25] A.A. Lerner, K.A. Cunefare, Performance of MRE-based vibration absorbers, J. Intell. Mater. Syst. Struct. 19 (5) (2007) 551–563.
[26] C. Bellan, G. Bossis, Field dependence of viscoelastic properties of MR elastomers, Int. J. Mod. Phys. B 16 (2002) 2447–2453.
[27] M. Farshad, M. Le Roux, Compression properties of magnetostrictive polymer composite gels, Polym. Test. 24 (2) (2005) 163–168.
[28] A. Boczkowska, S.F. Awietjan, R. Wroblewski, Microstructure–property relationships of urethane magnetorheological elastomers, Smart Mater. Struct. 16 (5) (2007) 1924–1930.
[29] A. Fuchs, Q. Zhang, J. Elkins, F. Gordaninejad, C. Evrensel, Development and characterization of magnetorheological elastomers, J. Appl. Polym. Sci. 105 (5) (2007) 2497–2508.
[30] M. Kallio, T. Lindroos, S. Aalto, E. Järvinen, T. Kärnä, T. Meinander, Dynamic compression testing of a tunable spring element consisting of a magnetorheological elastomer, Smart Mater. Struct. 16 (2) (2007) 506–514.
[31] A. Fuchs, J. Sutrisno, F. Gordaninejad, M.B. Caglar, L. Yanming, Surface polymerization of iron particles for magnetorheological elastomers, J. Appl. Polym. Sci. 117 (2) (2010) 934–942.
[32] J.-H. Koo, F. Khan, D.-D. Jang, H.-J. Jung, Dynamic characterization and modeling of magneto-rheological elastomers under compressive loadings, Smart Mater. Struct. 19 (11) (2010), 117002.
[33] G. Liao, X. Gong, S. Xuan, C. Guo, L. Zong, Magnetic-field-Induced normal force of magnetorheological elastomer under compression status, Ind. Eng. Chem. Res. 51 (8) (2012) 3322–3328.
[34] G. Liao, X. Gong, S. Xuan, Magnetic field-induced compressive property of magnetorheological elastomer under high strain rate, Ind. Eng. Chem. Res. 52 (25) (2013) 8445–8453.
[35] A. Martins, A. Fereidooni, A. Suleman, V.K. Wickramasinghe, Test rig development and characterization of magnetorheological elastomers, in: Proceedings of 25th AIAA/AHS Adaptive Structures Conference, Conference Jan, Conference, 2017, 0733.
[36] H. Vatandoost, M. Norouzi, S.M.S. Alehashem, S.K. Smoukov, A novel phenomenological model for dynamic behavior of magnetorheological elastomers in tension–compression mode, Smart Mater. Struct. 26 (6) (2017), 065011.
[37] K. Sapouna, Modelling, Characterization and Development of New Magnetorheological Elastomers with Enhanced Vibration Control Performance, Ph. D. thesis, University of Southampton, 2018.
[38] I. Agirre-Olabide, M.J. Elejabarrieta, A new magneto-dynamic compression technique for magnetorheological elastomers at high frequencies, Polym. Test. 66 (2018) 114–121.
[39] Y. Wan, Y. Xiong, S. Zhang, Temperature effect on viscoelastic properties of aligned magnetorheological elastomers under compression, Smart Mater. Struct. 28 (1) (2018), 015005.
[40] A. Bellelli, A. Spaggiari, Magneto-mechanical characterization of magnetorheological elastomers, J. Intell. Mater. Syst. Struct. 30 (17) (2019) 2534–2543.
[41] J.Y. Lee, V. Kumar, D.J. Lee, Compressive properties of magnetorheological elastomer with different magnetic fields and types of filler, Polym. Adv. Technol. 30 (4) (2019) 1106–1115.
[42] X. Shi, S. Liu, D. Zhao, Z. Zhao, J. Cui, F. Wang, Effect of electromagnetic force on dynamic mechanical properties of the magnetorheological elastomer under compression mode, J. Eng. Mater. Technol. 142 (2) (2020).
[43] A. Thorin, A. Azoug, A. Constantinescu, Influence of prestrain on mechanical properties of highly-filled elastomers: measurements and modeling, Polym. Test. 31 (8) (2012) 978–986.
[44] K.A. Kalina, P. Metsch, M. Kästner, Microscale modeling and simulation of magnetorheological elastomers at finite strains: a study on the influence of mechanical preloads, Int. J. Solid Struct. 102 (2016) 286–296.
[45] D. Ivaneyko, V. Toshchevikov, M. Saphiannikova, G. Heinrich, Mechanical properties of magneto-sensitive elastomers: unification of the continuum-mechanics and microscopic theoretical approaches, Soft Matter 10 (13) (2014) 2213–2225.
[46] Rubber, Vulcanized or Thermoplastic - Determination of Compression Stress-Strain Properties, 2017. ISO 7743:2017.
[47] Rubber, Vulcanized or Thermoplastic - Determination of Dynamic Properties - Part 1: General Guidance, 2011. ISO 4664-1.
[48] R. Brown, Physical Testing of Rubber, Springer US: Springer Science & Business Media, 2006.
[49] Standard Guide for Dynamic Testing of Vulcanized Rubber and Rubber-like Materials Using Vibratory Methods, 2011. ASTM D5992-96.
[50] R.H. Ewoldt, A.E. Hosoi, G.H. McKinley, New measures for characterizing nonlinear viscoelasticity in large amplitude oscillatory shear, J. Rheol. 52 (6) (2008) 1427–1458.
[51] E. Meinecke, S. Maksin, Influence of large static deformation on the dynamic properties of polymers, Colloid Polym. Sci. 258 (5) (1980) 556–563.
[52] Y. Fukahori, A. Hon, V. Jha, J. Busfield, Modified guth–gold equation for carbon black–filled rubbers, Rubber Chem. Technol. 86 (2) (2013) 218–232.
[53] S. Westermann, M. Kreitschmann, W. Pyckhout-Hintzen, D. Richter, E. Straube, Strain amplification effects in polymer networks, Phys. B Condens. Matter 234 (1997) 306–307.
[54] M. Klüppel, J. Meier, M. Dämgen, Modelling of stress softening and filler induced hysteresis of elastomer materials, in: Constitutive Models for Rubber IV, 2017, p. 171.
[55] J. Lejon, On the Frequency, Dynamic Strain Amplitude, Prestrain, Temperature and Magnetic Field Strength Dependence of Magneto-Sensitive Elastomers, Ph.D. thesis, KTH Royal Institute of Technology, 2012.
[57] J. Feng, S. Xuan, T. Liu, L. Ge, L. Yan, H. Zhou, et al., The prestress-dependent mechanical response of magnetorheological elastomers, Smart Mater. Struct. 24 (8) (2015), 085032.
[58] N.M. Wereley, C. Perez, Y.T. Choi, Strain-dependent dynamic compressive properties of magnetorheological elastomeric foams, AIP Adv. 8 (5) (2018), 056721.
[59] L. Peng, Z. Li, W. Luo, Y. Li, Analysis of dynamic viscoelastic properties of chloroprene rubber considering pre-strain effect, Mater. Res. Express 6 (10) (2019), 105324.

[60] Y. Han, A. Mohla, X. Huang, W. Hong, L.E. Faidley, Magnetostriction and field stiffening of magneto-active elastomers, Int. J. Appl. Mech. 07 (01) (2015) 1550001–15500016.

[61] Z. Xu, X. Gong, G. Liao, X. Chen, An active-damping-compensated magnetorheological elastomer adaptive tuned vibration absorber, J. Intell. Mater. Syst. Struct. 21 (10) (2010) 1039–1047.

[62] W.H.L.X.Z. Zhang, Adaptive tuned dynamic vibration absorbers working with MR elastomers, Smart Struct. Syst. 5 (2009) 517–529.

[63] D. Hao, D. Li, Y. Liao, A finite viscoelastic constitutive model for filled rubber-like materials, Int. J. Solid Struct. 64 (2015) 232–245.

[64] E. Guth, Theory of filler reinforcement, J. Appl. Phys. 16 (1) (1945) 20–25.

[65] M. Sadeghifar, R. Sedaghati, W. Jomaa, V. Songmene, Finite element analysis and response surface method for robust multi-performance optimization of radial turning of hard 300M steel, Int. J. Adv. Manuf. Technol. 94 (5) (2018) 2457–2474.